Inductively-coupled plasma optical emission spectroscopic determination of trace impurities in zirconium oxide-powder

KHAKHATHI LEONARD MANDIWANA

A dissertation submitted in partial fulfilment of

the requirements for the degree of

MAGISTER SCIENTIAE

in

CHEMISTRY

in the faculty of Science of the

UNIVERSITY OF PRETORIA

PRETORIA

SUPERVISOR: PROF CJ RADEMEYER

October 1996

MANDIWANA, KHAKHATHI LEONARD

INDUCTIVELY-COUPLED PLASMA OPTICAL EMISSION SPECTROSCOPIC DETERMINATION OF TRACE IMPURITIES IN ZIRCONIUM OXIDE-POWDER

MSc UP 1996

MANDIWANA KL

INDUCTIVELY-COUPLED PLASMA OPTICAL EMISSION SPECTROSCOPIC DETERMINATION OF TRACE IMPURITIES IN ZIRCONIUM OXIDE POWDER

MSc UP 1996

SYNOPSIS

Because of their extraordinary properties, advanced ceramic materials, eg. ZrO_2, offer new possibilities to science and technology in such important areas as microelectronics, high temperature applications in reactors and motors and also medicine. Due to these, Inductively Coupled Plasma Optical Emission Spectrometry (ICP-OES) has been used for the determination of the most significant impurities (Cr, Fe, U and Th) in high-purity refractory powders of ZrO_2 without matrix(Zr) separation. ZrO_2 powders were decomposed by fusion with a 10-fold excess of NH_4HSO_4 and subsequent dissolution of the melt in either HNO_3 or HF. ZrO_2 samples were fused and dissolved in both HNO_3 and HF. The results in the two acids were evaluated with respect to detection limits, blank values, interferences, accuracy and precision. The solution was then directly analyzed by ICP-OES, which was optimized for each independent analytical line. The calibration was performed by standard addition and matrix matching was not necessary.

The detection limits in ZrO_2 in the two acids varied from 1.73μg/l(Fe) to 50μg/l(U). The standard deviations obtained were 1-10% depending on the element and its concentration in the sample. There was no significant difference on the interferences and accuracy obtained in the two acids. The precision of the results in HNO_3 was poor as the results were not reproducible day after day due to precipitation. Except for Fe and Cr, the blank values encountered in HF were lower than in HNO_3, but generally

they were below the detection limits of the metals investigated. It was concluded that HF is the best acid to dissolve the fused ZrO_2 powders as it results in stable sample solution.

It was further investigated whether the presence of mineral acids, viz. HCl, HNO_3 and H_2SO_4, at 0-50%(v/v) concentration has significant influence on the emission signal of Fe as one of the impurities determined in ZrO_2. A number of solutions containing 1, 5, 10, 20 and 50μg/ml of Fe in acid concentrations of 0 to 50%(v/v) were used. It has been found that HNO_3 and HCl enhances the emission signal at low levels of Fe whereas H_2SO_4 depresses the emission signal of Fe at all levels. These effects are neither caused by the change in aerosol flow-rate nor the amount of aerosol reaching the plasma.

SAMEVATTING

Die buitengewone eienskappe van gevorderde keramieke soos ZrO_2, bied talle nuwe geleenthede vir wetenskaplike en tegnologiese ontwikkeling. Van die belangrike velde wat hierdeur geraak word is onder andere die mikro-elektronika, die ontwikkeling van sekere medisynes sowel as toepassings in hoë temperatuur reaktors as ook motorvoertuie. Die Induktief Gekoppelde Plasma Optiese Emissie Spektrometer(IGP-OES) is in hierdie studie gebruik om die belangrikste onsuiwerhede (Cr, Fe, U en Th) direk in baie suiwer, vuurvaste ZrO_2-poeiers te bepaal. Die ZrO_2-poeiers is eerstens deur smelting in 'n tienvoudige oormaat van NH_4HSO_4, ontbind. Hierna is die smeltsel in onderskeidelik HNO_3 of HF opgelos. Die oplossings is dan direk met behulp van die IGP-OES geanaliseer. Die instrument is vooraf vir elke analitiese lyn, afsonderlik geoptimiseer. Die standaard-addisie metode is gebruik vir kalibrasie en matrys passing was dus nie nodig nie. Die resultate is vervolgens geëvalueer ten opsigte van deteksie limiete, blanko waardes, steurings, akkuraatheid en presisie.

Die deteksie limiete wat vir die twee sure verkry is, het gewissel tussen 1.73 μg/l(Fe) en 50 μg/l(U). Afhangend van die betrokke element en sy konsentrasie, het die standaardafwyking tipies tussen 1-10% gevarieer. Daar is verder ook gevind dat die invloed van steurings en die akkuraatheid wat verkry is, nie betekenisvol verskil vir die twee sure wat gebruik is nie. Weens presipitasie, was die presisie wat van dag tot dag met HNO_3 verkry is, egter swak. Die blanko waardes wat met HF verkry is was,

met die uitsondering van Fe en Cr, laer as die van HNO_3. Die blanko waardes was egter oor die algemeen laer as die deteksie limiete van die elemente wat ondersoek is. Dit is gevind dat HF die beste suur was om die gesmelte ZrO_2 poeiers in op te los aangesien stabiele monster oplossings verkry word.

Die invloed van minerale sure, naamlik HCl, HNO_3 and H_2SO_4 op die emissiesein van Fe-onsuiwerhede in ZrO_2 is verder ook tot en met 'n konsentrasie van 50%(v/v) suur ondersoek. Oplossings met 1, 5, 10, 20 en 50 μg/l Fe in 0 tot 50%(v/v) suur is in die ondersoek gebruik. Daar is gevind dat HNO_3 en HCl die emissiesein versterk by lae vlakke van Fe. Hierteenoor onderdruk H_2SO_4 die sein by alle Fe-konsentrasies. Hierdie effekte is nie hoeveelheid aërosol wat die plasma bereik nie.

CONTENTS

ACKNOWLEDGEMENTS

I would like to thank my promoter, Prof CJ Rademeyer for his professional guidance, constant interest and encouragement in the course of this work, and for many fruitful discussions and suggestions.

I owe a great debt of gratitude to my parents, especially my late father for all the years of encouragement, moral support and the ambition he has built in me and for teaching me to believe in myself.

I also express a word of thanks towards the Foundation for Research Development for financially supporting me with a bursary.

Last but the not least I would like to thank my Creator for giving me the ability and providing me with the opportunity.

CHAPTER 1: INTRODUCTION

1.1 ICP as analytical method

Inductively Coupled Plasma Spectrometry (ICP-AES) is a technique used for the quantitative multielement analysis of biological and geological materials. The high temperature of the ICP allows the sensitive measurements of refractory elements such as B and P. The large dynamic ranges of ICP-AES make it possible to determine both major and trace elements from a single digest (i.e. percentage to μg/l range). For major elements the technique can provide good accuracy and precision if suitable calibration procedures and internal standardization are employed. Problems in the determination of trace elements can be related to the background enhancement and spectral line overlap from concomitant elements. Physical interferences in the nebulization process can also affect accuracy and precision. Internal standardization is often used to correct for sample transport variation.

Both Simultaneous and Sequential Inductively Coupled Plasma Atomic Spectrometry are in widespread use. Sequential systems have the advantage of flexibility in wavelength selection, which can be used to allow for variations in analyte concentration and matrix type, but the analysis time is necessarily longer. The complex composition of geological materials can give rise to several sources of interference in ICP-AES, but this can generally be minimized, if not eliminated, by

the use of one or more of the following: a high resolution spectrometer, on-line background compensation, pre-determined interference coefficients or matrix matched standards. An accurate method for background compensation can be achieved by scanning a spectral segment on either side of peak positions. The spectrum for each interferent is then measured, and its contribution is removed mathematically from the analyte signal.

1.2 Interferences

Even though the magnitude of matrix effects is smaller than the effects found with other excitation sources (flames, d.c. plasmas, microwave-induced plasmas and capacitively coupled microwave plasmas), significant matrix effects have been reported[1-3]. The matrix effect in an Ar ICP can be related to changes in the physical parameters of the solution and to the processes in the plasma itself. The most frequently studied matrix effects are those caused by easily ionizable elements(EIE)[4-6] and acids (organic and inorganic)[7-9].

Enhancement or depressant effect of EIEs on the analyte emission depends strongly on the operating conditions of the plasma, such as forward power, carrier gas flow-rate, observation height and the geometry of the torch. In addition to EIE's, a wide range of substances causes matrix effects in the Ar ICP. Moderate amounts of these substances can change the analytical signal significantly and these changes are

manifested as suppression or enhancement of the analytical signal. Thompson *et al*[10-12] showed that the different matrix elements produce changes in the sensitivity of both the atomic and ionic spectral lines. To account for the influence of the matrix on analyte emission, different parameters such as total excitation potential of the tested analyte line, decrease in excitation temperature, energy required to dissociate the matrix and ionization potential of the matrices were considered[12-14].

Inorganic and organic acids are commonly used for sample preparation, eg. extraction, digestion or dissolution, and consequently are major components of the sample matrix in many routine analyses. Usually, increase in the acid concentration results in a net line intensity reduction. This depression of intensity has been attributed to the following causes:-

- a change in the uptake rate because of a variation in the viscosity. This is usually observed with H_2SO_4 and H_3PO_4. In order to ensure the necessary analytical accuracy, the use of a peristaltic pump for forced nebulizer feeding, has been recommended in that case. However, the influence of great differences in viscosity of the solutions is only reduced but not completely removed[15].
- a change in nebulizer efficiency[16] and droplet size distribution because of both the viscosity and surface tension[17] variation. Although recent results indicate that the relationship of Nukiyama and Tanasawa equation[18] does not accurately describe the droplet size, the two terms of the relationship reflect the role of the viscosity and surface tension.

$$D_{3,2} = \frac{585}{V}\left(\frac{\delta}{\rho}\right)^{0.5} + 597\left[\frac{\eta}{(\delta\rho)^{0.5}}\right]^{0.45}\left(10^3\frac{Q_l}{Q_g}\right)^{1.5} \quad \text{.....(1)}$$

$D_{3,2}$ ≡ sauter mean diameter/μm

V ≡ the difference between the gas and liquid velocities/ms^{-1}

δ ≡ the surface tension/dyn.cm^{-1}

ρ ≡ the density of the liquid/g.cm^{-3}

η ≡ the viscosity of the liquid/poise

Q_l ≡ liquid flow-rate/cm^{3}s^{-1}

Q_g ≡ gas flow-rate/cm^{3}s^{-1}

This explains the signal reduction observed with H_2SO_4 and H_3PO_4 (at concentrations greater than a few percent) even with a forced uptake rate[19] but does not explain the signal reduction observed for HCl and HNO_3. These two acids do not exhibit any drastic variation in the viscosity and the surface tension as a function of the concentrations.

To overcome these acid effects, different correction methods were suggested:-

- matching the acid content of the standard solutions and the unknown solutions[17]. That seems easy to perform when both types of solutions are prepared in the laboratory. However, in particular with acid mixtures, this matching can be

made difficult when the acid concentration is not well defined.

- internal standardization[20]. Selection of the element to be used as an internal standard must be carefully performed in order to correct for this effect.
- correction can be done using the intensity of the H_β line[21], since this line intensity is proportional to the sample introduction rate. This correction has been reported as being efficient up to 55%(v/v) of HNO_3 for both atomic and ionic lines.
- simplex optimization of the ICP operating parameters (power, carrier gas, intermediate gas and outer gas flow rates) to minimize the acid effect, as demonstrated for 70% of acetic acid.

1.3 Aim of this investigation

The purity requirements of advanced ceramics are increasing owing to the dramatic effect of impurities on the physical properties of the resultant products[22]. Advanced ceramics is the family of ceramic materials which exhibits good mechanical, thermal, electrical, optical and (or) magnetic properties. They are suitable for high temperature engineering and electronic applications[23]. Some examples of advanced ceramics are Al_2O_3, SiO_2, Y_2O_3 and ZrO_2, and are produced by sintering or hot pressing of these refractory powders. The presence of impurities may influence these materials to loose their ability to chemical resistance, heat resistance, durability, strength and other properties. Consequently, the determination of impurities is an important step to

control (and maintain) the properties of these materials by controlling the impurity content.

The impurity levels in the compact ceramics are controlled by the quality of the raw materials. The resultant products formed from the raw materials are powders with strict requirements for particle size and particle size distribution and accordingly, they must have well-defined levels of purity[24]. ZrO_2 (commonly known as zirconia) is a hard solid with a high melting point of approximately 2700°C. The increasing technological interest in ZrO_2 based ceramics, eg. for manufacturing of laboratory crucibles, the lining of furnaces, a component of acid and alkali resistant glasses, use in electrical systems, corrosion-resistant hard tools and for oxygen-sensing makes a trace characterization of ZrO_2 powders used as their basic substances necessary[25]. For this reason, there is an increasing demand for more accurate and rapid methods of analysis.

Flame-excited atomic absorption spectrometry has been employed for the analysis of zircons but owing to the low levels of the trace components of these materials this technique is not suitable[26]. Ishii *et al*[27] developed a method whereby they used a high-resolution inductively coupled plasma atomic emission spectrometry method but they only managed to determine hafnium in high purity ZrO_2.

Min *et al*[28] describes the analysis of ultrafine ($d < 0.1\mu m$) ZrO_2 powders by slurry

nebulization ICP-AES. They proposed to use 40%(w:w) glycerine in 0.5mol/dm^3 HCl as a suspending medium. However, even for such extremely fine powders the slurries and solutions were found to behave differently in the ICP and the use of an empirically defined correction coefficient was mandatory. This makes the method of limited use for the analysis of real ZrO_2 powder samples. The commercially available samples of ZrO_2 powders usually have a grain size $>0.1\mu$m and the correction coefficient was found to depend on the type of the powder and on the element determined. Furthermore, the use of glycerine may introduce severe blanks for some elements.

The determination of trace impurities in ZrO_2 in ICP-AES has been reported[29] whereby samples were digested by fusion with NH_4HSO_4. Even though this fusion procedure is rapid and can be performed at low temperature and lower risk of contamination, the resultant samples prepared by dissolving the fused material in dilute HNO_3 were not stable as precipitates form within days of preparation which renders the method inactive and unsuccessful. In this study, a procedure has been developed whereby trace impurities (viz. Cr, Fe, Th and U) were determined in ZrO_2 without separating the Zr matrix by ICP-AES. Two independent acids were used (viz. HF and HNO_3) to dissolve the fused material. They were evaluated with respect to detection limits, blank values, %recoveries, interferences, accuracy and precision. In this procedure the calibration was performed by standard addition and matrix matching was not necessary.

1.4 References

1.1 Blades, M.W., and Horlick, G., Spectrochim. Acta, 1981, **36B**, 881

1.2 Moore, G.L., and Humphries-Cuff, P.J., and Watson, A.E., Spectrochim. Acta, 1984, **39B**, 915

1.3 Bambiro, F.O., Littlejohn, D., and Marshal, J., J. Anal. At. Spectrom., 1988, **3**, 279

1.4 Kawaguchi, H., Ito, T., Oto, K., and Mizuike, A., Spectrochim. Acta, 1980, **35B**, 199

1.5 Faires, L.M., Apel, C.T., and Niemczyk, T.M., Appl. Spectrosc., 1983, **37**, 558

1.6 Prell, L.J, Monnig, C., Harries, R.E., and Koirtyohann, S.R., Spectrochim. Acta, 1985, **40B**, 1401

1.7 Greenfield, S., McGeachin, H. McD, and Smith, P.B., Anal. Chim. Acta, 1976, **84B**, 67

1.8 Farino, J., Miller, J.R., Smith, D.D., and Browner, R.F., Anal. Chem., 1987, **59**, 2303

1.9 Xu, J, Kawaguchi, H., and Mizuike, A., Anal. Chim. Acta, 1983, **152**, 133

1.10 Thompson, M., and Ramsey, M.H., Analyst, 1985, **110**, 1413

1.11 Ramsey, M.H., Thompson, M., J Anal. At. Spectrom., 1986, **1**, 185

1.12 Ramsey, M.H., Thompson, M., and Walton, S.J., J. Anal. At. Spectrom., 1987, **2**, 33

1.13 Miller, M.H., Eastwood, D., and Hendrick, M.S., Spectrochim. Acta, 1984, **39B**, 13

1.14 Miller, M.H., Keating, E., Eastwood, D., and Hendrick, M.S., Spectrochim. Acta, 1985, **40B**, 593

1.15 Maessen, F.J.M.J, Balke, J., and De Boer, J.L.M., Spectrochim. Acta, 1982, **37B**, 517

1.16 Ishii, H., and Satoh, K., Talanta, 1983, **30**, 111

1.17 Wandt, M.A.E., Pougnet, M.A.B., and Rodgers, A.L., Analyst, 1984, **109**, 1071

1.18 Canals, A., Wagner, J., and Brower, F., Spectrochim. Acta, 1988, **43B**, 1321

1.19 Imbert, J.L., and Mermet, J.M., Analusis, 1984, **12**, 209

1.20 Myers. S.A., and Tracy, D.H., Spectrochim. Acta, 1983, **38B**, 1227

1.21 Botto, R.I., Spectrochim. Acta, 1985, **40B**, 397

1.22 Martinez-Lebrasant, C., and Barba, F., Analyst, 1990, **115**, 1335

1.23 Farinas, J.C., and Barba, M.F., J Anal. At. Spectrom., 1992, **7**, 869

1.24 Broekaert, J.A.C., Lathen, C., Brandt, R., Pilger, C., Pollmann, D., Tchöpel, P., Tölg, G., Fresenius J Anal. Chem., 1994, **349**, 20

1.25 Broekaert, J.A.C., Graule, T., Jenett, H., Tschöpel, P., Fresenius Z. Anal. Chem., 1989, **332**, 825

1.26 Bastius, H., Ceram. Forum. Int., 1984, 61, 3, 140

1.27 Ishii, H., and Satoh, K., Talanta, 1982, **29**, 243

1.30 Min, H., and Xi-en, S., Spectrochim. Acta, 1989, **44B**, 957

1.31 Lobinski, R., Broekaert, A.C., Tschöpel, P., and Tölg, G., Fresenius J Anal. Chem., 1992, **342**, 569

CHAPTER 2: INDUCTIVELY COUPLED PLASMA OPTICAL EMISSION SPECTROMETRY (ICP-OES)

2.1 The theory of ICP-OES

ICP-AES is based on the principle that excited atoms and ions emit radiation of characteristic wavelength when their electrons return from excited to ground state. The identification of the wavelength present in the spectrum permits qualitative analysis whereas the intensity permits quantitative analysis of the sample.

Figure 1 Schematic representation of ICP-AES structure

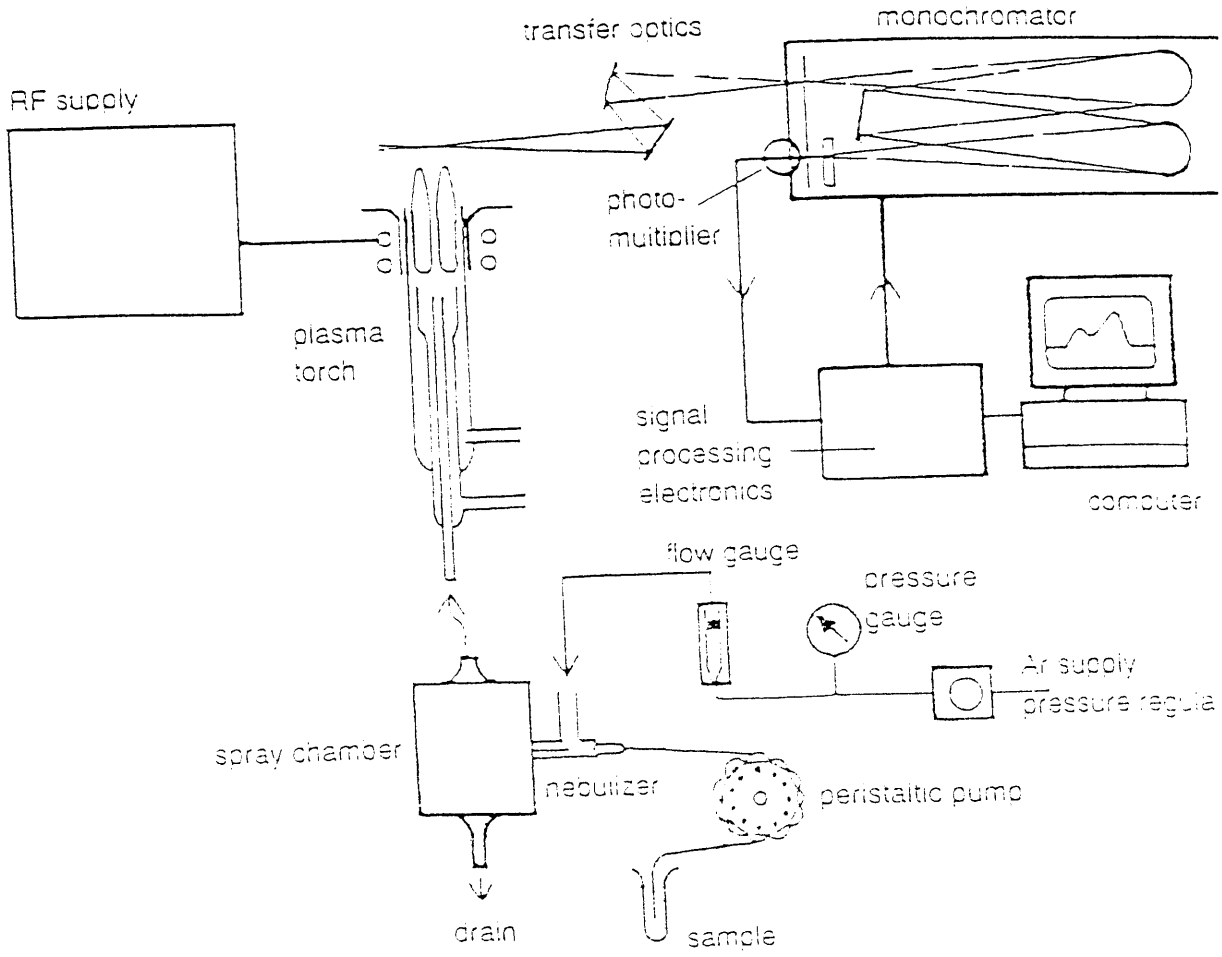

Figure 1. The components of an ICP atomic emission spectrometer

A typical arrangement for ICP-AES is shown in figure 1 and consists of:-

- A sample introduction system
- The ICP torch and its associated gas supplies
- A radio-frequency generator
- An optical spectrometer
- Detectors and associated electronics
- Computerized instrument control, data collection and analysis

The sample to be analyzed may be in the form of solution, gas, solid or slurry. Samples are introduced into the ICP, mostly in solution form, after being prepared by a process called digestion or fusion procedure. It is preferable to prepare the sample in this way so as to eliminate or minimize interferences due to sample matrix and to improve high detectability of the analyte elements by destroying the organic matrix. Nebulizers are undoubtedly the most common means of liquid sample introduction. Sample solutions are delivered to the nebulizer tip with the aid of a peristaltic pump. The nebulizer converts the liquid sample with the aid of Ar gas to aerosols, which is then transported to the plasma. Before the aerosols reaches the plasma, large droplets are filtered out in the spray chamber to avoid uneven distribution of the different analyte elements between droplets of different sizes.

There are two classes of nebulizers: Pneumatic and non-pneumatic. The term "Pneumatic" refers to the use of compressed gas to generate aerosol. Pneumatic

nebulizers for ICP spectrometry may be divided into several broad categories, of which the most important are concentric, cross-flow and V-groove. Each of these categories contains many different versions of the basic design and it will not be appropriate to discuss them here. All-glass pneumatic nebulizers show a tendency to produce droplets of decreasing average droplets size when the nebulizing gas flow rates are increased[2]. The main problem associated with pneumatic nebulizers is blockage of the narrow sample solution capillaries by solutions containing high percentages of dissolved solids or suspended particulates. This can lead to erratic performance and low emission signal.

Non-pneumatic nebulizers, eg. ultrasonic nebulizers, rely on the energy of a high velocity gas (e.g. Ar) to nebulize a liquid. Ultrasonic nebulizers apply energy to the liquid with a piezoelectric transducer driven at ultrasonic frequencies. This has the advantage of making the generation of aerosol independent of the flow rate of the gas transporting the aerosol into the plasma, so the two parameters can be optimized independently. More importantly, the efficiency of aerosol generation is typically up to ten times better than that of convectional pneumatic nebulizers[3]. Consequently, the sensitivity is greatly improved. Ultrasonic nebulization suffers from the drawback of greater memory effect following the aspiration of a solution containing a high concentration of the analyte[4]. As ultrasonic nebulizers offer higher sample throughput time, pneumatic nebulizers, with the lesser memory effects are usually employed in routine analysis.

The plasma is formed in a fused-silica torch (see figure 2a) consisting of three concentric tubes (mainly made of quartz) through which streams of Ar flow. Surrounding the top of this tube is a water-cooled induction coil connected to a radio frequency (RF) generator. To understand the nature of the plasma, it is essential to remember three simple facts: by definition, plasmas are gases in which a significant fraction of their atoms or molecules are ionized, that being so, magnetic fields may readily interact with plasmas, and one of these interactions is an inductive coupling of time-varying magnetic fields with the plasma, analogous to the inductive heating of a metal cylinder[5]. Energy is transferred into the ICP by the interaction of ionized Ar with the electromagnetic fields of the induction coil. These magnetic fields are formed in such a way that the high frequency currents flowing in the induction coil generate oscillating magnetic fields whose lines of force are axially oriented inside the (quartz or silica) tube and follow elliptical closed paths outside the coil as shown in figure 2(b).

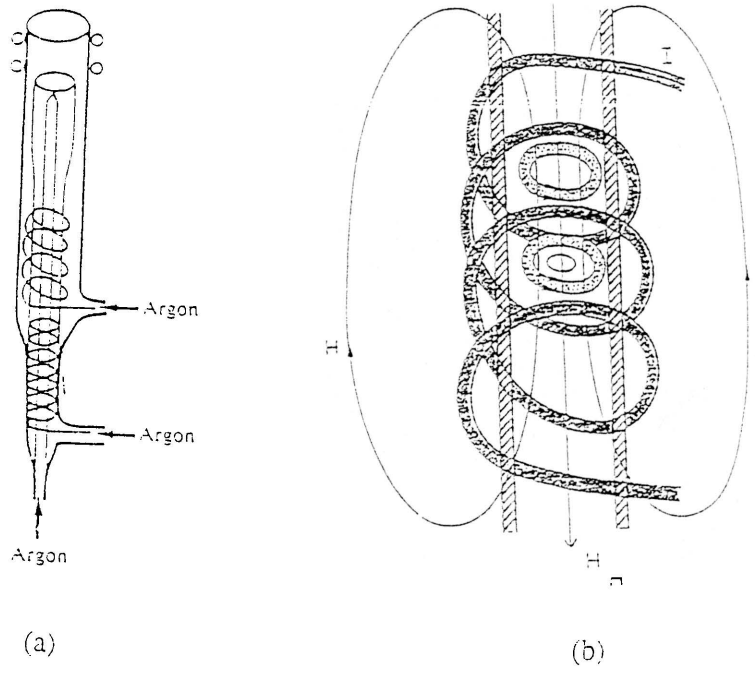

Figure 2: (a) Plasma torch[5]
(b) Magnetic fields and eddy currents generated by induction coil[5]

The positive Ar ions and the electrons are both accelerated by the high frequency field of the coil, but because of their far smaller mass the electrons are accelerated to much higher velocities than the ions and energy transfer into the plasma is dominated by processes involving electrons. When a spark is passed through Ar in the presence of the RF field of the induction coil to initiate the plasma, some electrons in the spark gain sufficient energy to undergo inelastic collisions with Ar atoms. An energetic electron colliding with an Ar atom may transfer enough energy to ionize the Ar, releasing another electron which is available to participate in the transfer of energy from the coil to the gas. A steady-state plasma is produced when the rate at which electrons are released by ionizing collisions equals the rate at which they are lost by recombinations. Ion-electron recombinations emit light, producing a continuous spectrum corresponding to the distribution of ion kinetic energies in the plasma.

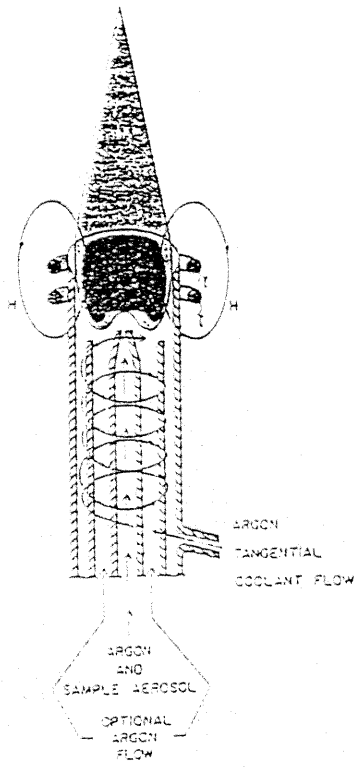

Figure 3. Complete plasma configuration[3]

The plasma formed as explained above attains a gas temperature of 5000 - 10 000K in the region of maximum eddy current flow. At these temperatures it is desirable to provide some thermal isolation of the plasma to prevent overheating of the quartz containment cylinder. This isolation is achieved by Reed's vortex stabilization technique[7,8], which utilizes a flow of Ar that is introduced tangentially in the manner shown in figure 3. The tangential flow of Ar streams upward, cooling the inside walls of the outermost quartz tubes and centering the plasma radially in the tube. The plasma itself is anchored near the exit end of the concentric tube arrangement. Apart from Ar being used for the formation (or initiation) and thermal isolation of the plasma, it also transports the sample to the plasma as an aerosol. Ar is also used as the auxiliary gas which raises the plasma relative to the torch and prevent salt build-up on the tip of the injector tube.

The frequency supplied by the RF generator determines the type of the plasma which will be formed[9]. If the plasma itself is generated at lower frequency ($\sim$5MHz), tear-drop shaped plasma, as shown on the left portion of figure 4, tends to be formed. Sample material that approaches the plasma tends to follow a rather disconcerting path around the outside surface and not penetrating the centre. As shown in the highly schematic form on the right-hand portion of figure 4, an increase in oscillating frequency of the power source causes the eddy current to flow more closely to the outer or skin portions of the plasma. In this way, an incipient annula plasma has the appearance of a doughnut. Since the hole possesses a somewhat lower temperature

than tear-drop, it offers less resistance to the injection of the sample material. Apart from this, annula plasma, allows penetration of the aerosol carrier gas through the centre of the plasma.

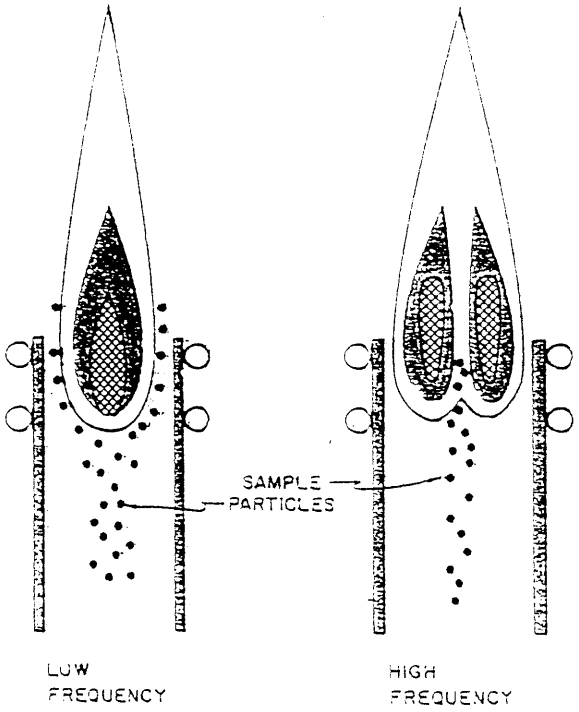

Figure 4. Sample particle paths for several plasma shapes[3]

The plasma has the appearance of a very intense, brilliant white, non-transparent core topped by a flame-like tail. The plasma core, which resides insides and extends a few millimetres above the load coil region, emits an intense continuum in addition to a rather fully developed spectrum of neutral argon. The continuum presumably arises from ion-recombination process and bremsstrahlen emission. When solutions of certain elements (eg. Yttrium) are introduced, the emission of visible light allows the various zones in the axial region of the ICP to be viewed directly[10]. The central channel of the

plasma, which is of little analytical interest consists of the pre-heating zone (PHZ), the zone where desolvation, evaporation and dissociation takes place. This zone is followed by the initial radiation zone (IRZ) and the normal analytical zone (NAZ) where analytical atoms begin to emit and spectral emission is primarily from ions for most elements respectively. As the majority of elements emit most intensely in NAZ, this zones is used for most elements. The tail-flame appears above the NAZ and is barely visible when distilled water is nebulized but assumes typical flame colours when analytes are added to the plasma.

The function of the radio frequency (RF) generator is to supply an alternating current at a desired frequency to the induction coil which is used to form and sustain the ICP. Currently, there are two types of generators, referred to as "free running" and "crystal controlled". A "free running" generator allows the frequency of the oscillating current to vary as the impedance of the plasma changes. The "crystal controlled" generator maintains constant frequency regardless of the plasma impedance due to the presence of a piezoelectric crystal. It usually operates in the low milliwatt output range, as the crystals cannot carry large currents. The higher frequency modulation of the RF generator results in both high precision of analysis and enhanced signal to background ratio. Water cooling of the power tube ensures the maintenance of the RF generator's stability.

The photomultiplier tube of the spectrometer converts the light intensity into an

electrical signal that can be quantified and related to the concentration of the particular element in solution. There are two types of spectrometers available, viz.simultaneous and sequential scanning spectrometers. The simultaneous spectrometer uses an array of detectors to measure a number of lines (channels) at the same time. A sequential system measures one element after another giving an unrestricted choice of wavelength to be measured. A productive spectrometer must be able to fulfil the following capabilities:-

- it must provide a high degree of resolution to achieve good separation from nearby spectral lines, thus minimizing inter-element interferences
- it must exhibit excellent light gathering capabilities and minimal stray light to ensure good sensitivity
- it must be mechanically and thermally stable to ensure both the precision of the analysis and the ability to locate the correct analytical line.

The advantages and disadvantages of ICP-AES as an analytical, spectroscopic tool are summarised here below. Compared with flames or graphite furnaces, species in an ICP is much more highly excited due to the high temperature. Excited states are so extensively populated in the ICP that intense emission is produced from many lines simultaneously. As a result, rapid simultaneous analysis can be performed. Emission from a flame or graphite furnaces is much less intense - characteristic of temperatures between 2000 and 3500K. Absorption spectrometry is used to detect atoms in flames or graphite furnaces that absorbs light involving excited states with low energies of <3eV (Na, K, Ca and Li).

ICP-AES offers low detection limits (μg/l or less for some elements) because of their large emission signals and small background as detection limits are often determined from the relative magnitudes of the signal and the noise of the background. Detection limits obtained in ICP-AES are sample dependent and are degraded if background increases or spectral overlaps are present. For example, if the interference has an intensity that is 10 times the background intensity at the analyte peak, the practical detection limit will be degraded by about a factor of 10, assuming that the relative standard deviation (RSD) of the interfering species is equal to that of the background[11].

Some matrix effects (e.g. atomization and excitation interference effects) in ICP-AES are smaller than in flames or graphite furnaces. One source of these matrix effects in flames and furnaces is incomplete atomization, particularly of refractory species such as oxides. In the ICP, two factors tend to minimize this type of matrix effect: a more "inert" environment and higher temperatures. However, the ICP is not totally inert. Sample water vapour and aerosol produce a concentration of oxygen atoms in the plasma, roughly 2 x $10^{16}cm^{-3}$, that is similar to the concentration of oxygen atoms in flames.

The high temperature consistent with intense emission and minimal vaporization-type matrix effects also produces one of the biggest problems in ICP-AES: spectral overlap[12]. Based on Wohlers'ICP wavelength tables[13], an average of 294 spectral lines

are emitted per element depending on the temperature, ranging from eight for H to 2532 for Cs at wavelength between 183 and 850nm. Rare-earth elements, which were not listed in Wohlers' tables, produce notoriously cluttered spectra. The wide linear dynamic range characteristic of ICP-AES allows measurement of trace quantities of one analyte and major quantities of another simultaneously without sample dilution, separation, or preconcentration. Very weak emission intensities, however, must be measured in the presence of intense emission from other elements. Further, lines from different elements have widely varying sensitivity. For example, sensitivity for the most intense Ca and Sn lines differ by a factor of 5000. If a sample contains 1μg/ml Sn and 1000μg/ml Ca, the Sn line intensity is 5 x 10^6 times less intense than the Ca line.

Direct line overlaps, broadening of spectral lines, and stray light can also produce overlap problems. However, ICP-AES is very selective when interference free spectral lines can be found. It is possible to determine sub-part-per-billion levels of some elements in the presence of up to 10 000μg/ml of other elements. Spectral interference can be minimized (but not eliminated) by using high-resolution spectrometers.

Although many matrix effects (eg. interferences from easily ionizable elements) in ICP-AES are in general less severe than those encountered in flames and graphite furnaces, the severity of these problems is strongly dependent on its origin. Formation of molecular refractive species is less severe in ICPs than flames. However, at high

concentrations almost every matrix can cause a change in sensitivity[14]. Errors can be produced by dissolved solids as well as solvents (acids or organic solvents)[15-17], and matrix effects can originate in the aerosol generation and transport process or in the plasma itself. However, according to equilibrium calculations, all elements with ionization potentials $<8eV$ should be more than 90% ionized in the analytical zone of the ICP. The nature of the matrix induced error (including whether it enhances or depresses the signal) is highly dependent on experimental conditions (gas flow rates, applied power, etc) and the point at which the plasma signals are measured. Low in the plasma, concomitant species produce increased emission intensities and high in the plasma, depression are normally observed.

It can therefore be concluded that ICP has\will become the dominant source for rapid spectroscopic multielement analysis as a set of "legendary" attributes, including low detection limits, a wide linear dynamic range, and high precision.

2.2 Interferences in ICP-OES

2.2.1 Introduction

Inductively Coupled Plasma Emission Spectrometry (ICP-AES) has become accepted as the contemporary method of choice for multi-element analysis. Early reports described ICP as virtually free from interferences[18]. While the ICP is certainly

superior to most, if not all other spectroscopic sources in this respect, subsequent studies have shown that interferences do exist in the ICP, and can at times be quite severe. Although many researchers have studied these interferences (sometimes called matrix effects) there is no consistency in the data presented (may be attributed to the different operating conditions) and there is no fundamental explanation for the observed effects[19]. There are in addition, other types of interferences that can cause problems when real samples are analyzed by ICP-AES, viz. transport interferences, solute volatilization interferences, etc.

A matrix effect is a phenomenon which occurs when a matrix constituent present in a sample affects the emission intensity measured for the analyte. These interferences may be divided into two categories, viz. spectral or non-spectral. Spectral interferences are dependant on the spectral bandwidth of the spectrometer and spectral characteristics of the analyte and the interferent. These spectral interferences are not considered in this study because they are controlled by the design of the spectrometer. Non-spectral interferences may further be classified by processes such as nebulization, volatilization, shift in ionization equilibrium, atomization, excitation, energy and mass transport, etc. None of these processes can individually explain the whole effect[20].

As chemical interferences are caused by the presence of certain elements (or compounds) at certain concentration(s) such that they prevent the accurate

measurement of the determined species, eg. the presents of sodium in a sample at certain levels enhances the emission signal of both the alkali and alkali earth metals[21], it is very important to identify and characterise these interference effects since the accuracy of an analysis can be affected by these effects.

2.2.2 Sources of interferences

The sources of interferences due to matrix effects in ICP-AES are caused by the sample introduction system and the excitation source.

2.2.2.1 Sample introduction system

When the ICP-AES technique was introduced, nebulization, transport and desolvation interferences had been corrected through the introduction of the peristaltic pump and spray chamber which assures the introduction of the sample at a constant rate on an even distribution of analyte elements into the plasma. The effects of variation in the concentration or the nature of the acid medium of the analyte sensitivity has been established. Such effects can be corrected by standardizing the acid concentration in the test solution for both samples and standards[22].

2.2.2.2 Excitation Source

The source of matrix (interelements) effects on the analyte emission intensity had been found to be influenced by the presence of ionization interferences in the ICP. These interferences were expected to occur through changes in either or both the electron number density or electron temperature as in various sources like the combustion flames of the dc arc through the introduction of the concomitant species[23]. Ionization interferences are more influenced by the shape of the plasma.

2.2.2.2.1 The shape of the plasma

The annula (doughnut) plasma which is toroidal in shape is favoured over the tear-drop shaped plasma. It provides the following advantages which are shortcomings of the tear-drop plasma:-

- it allows efficient sample introduction
- it allows penetration of the aerosol carrier gas through the centre of the plasma.

In a tear-drop plasma, the sample has a tendency to flow around the outer surface of the plasma, not penetrating the centre. In this case, the presence of the concomitant species in the sample would change the plasma impedance resulting in a change in energy density coupled into the plasma, leading to apparent ionization interferences.

2.2.2.2.2 Operating parameters of the ICP

Operating conditions which seem to influence ionization interferences are :-

(i) Observation height

(ii) aerosol carrier gas flow-rate

(iii) incident power

These three parameters, which are interdependent, are correlated with the position of the initial radiation zone(IRZ), the zone where ionization interferences occurs. The position of the IRZ is also coupled with the residence time of the sample in the plasma, where the residence time is determined by the observation height and the carrier gas flow-rate.

Ionization interferences normally occurs at the position low in the plasma, meaning low observation height at normal carrier gas flow and increasing higher with increasing carrier gas flow. The IRZ can be shifted by changing the following parameters:-

(i) increase in carrier gas flow shifts the zone upwards

(ii) increase in incident power shifts the zone downwards

Ionization interferences could be eliminated by keeping the observation height fixed while changing the other two parameters[24].

2.2.3 Easily ionizable elements (EIE) and non-easily ionizable elements (NON-EIE) matrix effects in ICP

The presence of EIE's (eg. Li, Na, K, or Cs) and NON-EIE (esp. Ca) in the sample at certain levels either depresses or enhances the emission signal of the determined analyte element. The order of enhancement have been shown to be related to the ionization potential of the matrix element. This enhancement is higher for concomitant elements of lower IP and decreases in magnitude as the IP of the matrix increases[17]. This has been explained in detail in 2.2.4.

2.2.4 Factors suspected of causing matrix effects

2.2.4.1 Solution transport efficiency and mean sauter droplet

The physical parameters of the solution being analyzed can affect the rate of transport of the analyte solution to the nebulizing tip. This may be caused by an increase in the density of the concomitant species. The overall results of increasing the amount of the matrix element will be an increasing depression of the emission signal as the amount of the analyte reaching the plasma decreases.

Different physical parameters of the solution may also cause a volatilization effect. In this case, analyte atoms are included in the dissolved particle matrix which could

require longer time to be volatilized than analyte particles alone. This might be possibly due to different particles sizes. For these reasons, the relevant physical parameters, such as density, viscosity and surface tension, of solutions with different concentration of the matrix element must be measured. It is evident that there are some differences in solution properties, which may cause, to some extent, differences in the method of introduction of the solution into the plasma and in the atomization and transport of particles to the ICP.

Applying the Nukiyama and Tanasawa equation[25] (see 1.2), the sauter mean diameter of the droplets, $D_{3,2}(\mu m)$ may be estimated for various solutions.

An increase in the mean drop size of the primary aerosol will generally result in a reduction of the analyte mass transport to the plasma and hence to a reduction in emission signal. It should be mentioned that in spite of restrictions of the validity of this equation, it is frequently used in the literature to at least predict trends in the mean drop sizes of the aerosol, only in that sense, should this equation be used in a report. According to the experimentally determined physical properties of the solutions investigated, Tripkovic *et al*[19] have shown that within the error limits, there is minor differences in the values of the sauter mean diameter of a pure water and solutions containing Li and Zn.

The enhancement factors obtained for various analytes indicates fairly different behaviour of the atomic and ionic lines of the same analyte in the presence of different matrices. If the presence of the matrix changed the nebulization efficiency and resulting sauter mean diameter considerably, then different amounts of the analytes, with altered droplet size distribution of aerosol would reach the plasma and change the desolvation, volatilization and enhancement or depression of analyte emission signal.

2.2.4.2 Increased excitation of analytes by electrons from EIE

It has been shown that enhancement caused by EIE low in the ICP are primarily due to increased excitation of the analyte emission signal. This increased excitation is not accompanied by an increase in apparent excitation temperature[19,26,27].

The induction zone or toroid of the plasma is a region of high electron and Ar ion concentration because of its high temperature. The central channel is a cool region of low electron and ion density with a reasonably well defined boundary. In the central channel, the analyte is normally present at low concentration and it creates few ions and electrons. The analytes travels up the central channel interacting relatively little with the plasma mainly receiving thermal excitation. When an easily ionizable element is present, it supplies a source of low energy electrons in the central channel. These electrons can cause additional analyte excitation, but more importantly they exchange with electrons from the induction region of the plasma[26]. This reduces the inhibition

of diffusion of toroid electrons to the central channel. The proposed mechanism is consistent with increased excitation of atoms and ions in the presence of EIE matrix and it is non-thermal.

2.2.4.3 Change in emission efficiency

If the claim (by some reporters that there is no change in electron number density[28-29] nor in spatial distribution[30] of the analyte species during the formation of interferences in the presence of EIE) of EIE is true, then EIE may in some way affecting the efficiency of the analyte emission. As the upper excited states of the ICP has higher populations, then collisional deactivation in those states are likely to be a radiationless process because the ICP is not in thermal equilibrium. This could alter the emission intensity without changing the measured excitation temperature noticeably. An increase in the radiationless processes results in the suppression of the emission intensity. Emission efficiency is influenced by collisional quenching[31]. Though Ar atoms, ions and electrons are likely to take part in the deactivation process, Ar atoms are therefore not involved due to their small quenching cross-sections. In contrast to this, Wu *et al*[32] have determined the effects of EIE on the emission efficiency of the analyte. They have proved from theoretical and experimental results that emission efficiency does not change significantly in the presence of EIE, and that radiationless excited-state energy loses by free electrons are not major reason for the effect in the ICP-AES.

2.2.4.4 Shift in ionization equilibrium

An increase in the electron density of the plasma would shift the equilibrium toward neutral atom species resulting in enhancement of atomic emission and depression in ionic emission[33]. The degree to which this mechanism will influence emission intensities in the plasma will depend upon how much the electron number density in the plasma is changed by the introduction of EIE. Calculations[34] and measurements[19,35] show that electron density does not change significantly when sodium was introduced into the solution. However, the measurement of electron density extended only from 15mm to 25mm above the load coil. An extrapolation of the plot of electron density as a function of observation height to lower regions indicates that this may not be the case between 0 and 15mm above the load coil.

2.2.4.5 Ambipolar diffusion

Boumans *et al*[36] have mentioned ambipolar diffusion as a possible source of emission intensity modification in the ICP. Ambipolar diffusion is defined as the diffusion of charged particles under the influence of an electric field[37]. In a gas which contains a quantity of ions and electrons, electrons tend to diffuse faster than ions and that is related to their smaller mass. The resultant separation of charge produces an electric field which exerts its force in such a way as to increase the drift velocity of the ion species and retard the drift velocity of electrons. Neutral particles may be left

unaffected by this process to the extent that their population is not coupled by an ionization equilibrium to that of ions. The diffusion is in the direction from higher to lower electron densities. Murayama *et al*[38,39] have interpreted the enhancement of emission from rare earth elements in a microwave discharge as a results of ambipolar diffusion.

2.2.4.6 Volatilization effects

Kornblum *et al*[40] discussed the possibility of volatilization effects in the ICP as a mechanism to explain the effects observed due to EIE's. In this mechanism, analyte atoms are included in a desolvated particle matrix which may take longer time to volatilize than analyte particles alone. This may either be the result of larger particles, or particles with atomic bonds which are more difficult to break. The net effect is a delay in the release of the analyte atoms, when compared to the situation without matrix. This delayed volatilization can result in shifts in the spatial behaviour of the analyte emission. In the ICP, a lateral diffusion effect would most likely result in a depression of emission in the central zone of the plasma, and enhancement nearer the edges of a radial analyte distribution, in lower regions of the analyte channel. Shifts in radial emission profiles[41] in the ICP have been explained as due to volatilization effects.

2.2.4.7 Radial and vertical position of the plasma

Both EIE and NON-EIE have a large effect on the emission intensities in the ICP when present at higher concentration (~ 0.05M)[42]. The magnitude and direction of the matrix effects are strongly dependant on the radial and vertical position in the plasma. Largest depression of the emission intensities occur in the centre of the plasma and tend to be severe for less easily ionizable elements. Enhancement tend to occur off-axis and are largest for EIE. At some height in the ICP, matrix-induced depressions of the emission intensities in the centre is equal to enhancement off-centre. Ion emission intensities measured as a line-of-sight data from the side of the ICP are less affected by the presence of concomitant species than one would expect on the basis of the concentration of ions in the plasma measured by laser induced fluorescence.

There are two reasons for the less severe matrix effects in the ICP-AES. First, while the number of ground state ions are decreased in the presence of matrix elements, more analyte ions are excited. These two effects compensate for each other. Secondly, line-of-sight intensities tend to change less than the intensities in the radial centre of the plasma. Off-axis enhancement compensate for on-axis depressions in emission intensities.

2.2.4.8 Inefficient atomization, excitation and ionization

The ICP is a source where it is possible to combine atomization of the sample, excitation and ionization of the free atoms. The high kinetic temperature exhibited by the plasma, usually greater than 5000K should permit complete atomization of any type of the sample to be observed. As the atomization process involved are of the same order of time as the residence time of the sample, i.e. a few seconds, complete atomization and efficient ionization (i.e few nanoseconds) will be obtained only if careful optimization of the ICP operating parameters is done.

The important parameters are the carrier gas flow-rate and inner diameter (i.d) of the injector tube. The velocity of the cold gas at the exit of the injector is dependent on both the carrier gas flow-rate and the i.d of the injector tube, whereas the amount of the aerosol going to the plasma depends on the carrier gas flow-rate. A reduction of power also reduces the energy-transfer. As for the optimization of the atomization and ionization, interference effects such as those produced by the addition of EIE, can be minimized with the same set of parameters. A simple way to verify this optimization is to use an ionic to atomic line intensity ratio of an element. It was seen that Mg is suitable for this purpose. Values of the MgII 280.27nm/MgI 285.21nm line intensity ratio above 10 correspond to an optimization of the ICP and minimization of interferences effects caused by the presence of EIE[43]. A theoretical ratio is calculated assuming local thermodynamic equilibrium.

2.2.4.9 Formation of metal-metal complexes

The enhancement of atomic and ionic signal in the presence of EIE may be caused by the increase atomization of the molecular species. This is conceivable because analyte atoms may associate with the concomitant element to form metal-metal complexes instead of oxides or hydroxides during desolvation and vaporization in the plasma[44]. Since the analyte-EIE association is commonly weaker than the analyte-oxygen bonding, atomization is facilitated in the presence of large amounts of EIE.

2.2.4.10 Enhanced collisional excitation, ionization potential (IP), excitation potential (EP) and matrix concentration

Veillo *et al*[45] suggested that enhancement in emission intensity may be due to increased collision rate due to an increase in electron density. This mechanism was used to explain the increases in emission intensity due to the added Na, which did not cause corresponding increases in the ground state population of the analyte species. Franklin *et al*[46] suggested that this could be used to explain simultaneous enhancements in the emission intensity from both the ion and atom lines (eg. Ca) in an ICP.

The ionization potential of both the analyte and the concomitant has an effect on the amount of enhancement or depression of the analyte intensity. The lower the IP of the concomitant species, the higher is the degree of enhancement of the analyte emission

signal. An analyte element with low IP is enhanced more than the one having higher IP in the same matrix as less energy is needed for the formation of ions. These effects also applies for matrix and analyte elements having low EP. The matrix concentration also has a major effect on the emission signal of the analyte. The enhancement of the analyte emission signal is significant for high matrix concentration[19].

2.2.5 Matrix effects determination in the analysis of geological and biological samples

In the following paragraphs some examples are presented where the interferences discussed in 2.2.4.1 - 2.2.4.10 have been determined in the analysis of real samples.

2.2.5.1 Matrix effects in Ar Plasma on elemental analysis of archaeological glazes by Inductively Coupled Plasma Atomic Emission Spectrometry

Matrix effects of Lithium

It is known that EIE may shift the ionization equilibrium in the plasma and hence affect the sensitivity of the elements determined. Paama *et al*[47] has investigated the effect of Li (50 - 600μg/ml) which was one of the constituent of the fusion flux used to digest archaeological glazes. Li (50 - 600μg/ml) was added to a standard solution containing 1.00μg/ml Al, Ca, Cu, Fe, Mn and Zn, and 2.00μg/ml of Pb and Si. The

influence of the matrix of $Li_2B_9O_7$ on the intensities of the ion and atom lines was investigated.

The lines were affected according to their excitation potential (EP) for the atom lines and the EP plus the ionization potential (EP + IP) for the ion lines, see 2.2.4.10. The Li added had only a minor effect on the concentrations measured and simple aqueous standards could be used for calibration. The concentrations of the major elements in the analyzed solution were, 10 - 150μg/ml, and Li did not have a significant effect as its actual concentration in the fused sample was approximately 330μg/ml

Influence of a matrix of metallic ions on the B I 249.678nm line intensity

Various concentration of the Si, Al, Fe, Mn, Pb and Cu matrix (0-600μg/ml) on the 1.00μg/ml BI emission signal at 249.678nm line were studied. The relative intensities of the B I 249.678nm line, measured in the different matrices was 6% for Si concentrations of up to 500μg/ml and was less than 5% for the other elements. As the concentrations of Si, Na, Al, Fe, Mn, Pb and Cu in the fused RMs and glazes samples were $<$ 200μg/ml, thus, they have no significant effect on the B emission signal. The validity of this analytical method was tested by analysing US Geological Survey RMs and glazes standards which were found to be in good agreement with the certified values[48].

From this investigation, the ICP-AES technique had been proved to be suitable for elemental analysis of glazes. Sample decomposition was achieved by fusion with $Li_2B_4O_7$ and it was possible to measure directly both the main and minor elements of the samples. Chemical and Spectral interferences were not encountered and ionization interferences were neglible, although the samples contained high levels of Al, Pb, Si and Fe.

2.2.5.2 Emission efficiency for particulate forms of iron and Aluminium in rain-water measured by Inductively Coupled Plasma Atomic Spectrometry

The emission efficiency for particulate forms of Fe and Al in rain-water was evaluated by Ambe *et al*[49] using ICP-AES. When samples were directly introduced into the ICP spectrometer, a significant difference in the emission intensity of various elements was observed in filtered and unfiltered samples, suggesting this difference could be applied to estimate forms of elements in rain-water.

The emission efficiency was defined as $100(C_d-C_f)/C_p(\%)$, where C_d is the emission intensity of an element in unfiltered rain-water measured by direct sample introduction into the ICP and expressed as concentration of the element (μg/ml), C_f is the emission intensity of the element in the filtered rain-water (μg/ml) and C_p is the concentration of the element in particulate matter measured after digestion (μg/ml). Emission

efficiency was calculated for the samples filtered through each pore size of filter. According to this definition, the emission efficiency express the total efficiency of the ICP system with regard to the emission of the particulate matter, including the efficiency of sample introduction, transport particles in the nebulizer and mixing chamber, the fraction of the atomized analyte in the plasma, etc.

Various particle sizes, viz. >8, 1 - 8, 0.4 - 1 μm, of rain- water were collected by filtering through a filter of the equivalent size. From the results, it was found that the emission efficiency of Fe and Al decreased with increasing particle size. The emission efficiency of Fe was usually a little higher than that of Al for every particle size which agrees well with the order of ease of atom formation[50]. This emission efficiency for these elements include, not only efficiency of atom formation in the plasma but also many factors, such as the efficiency of the nebulizing process. The combined effects of these process are considered markedly to decrease the value of emission efficiency for larger size particles.

The concentration of Fe and Al in various sizes of particles in rain-water was estimated by dividing the difference in emission signal between the filtered and unfiltered rain-water by the emission efficiency of each size. The major proportion of the particulate form of Fe and Al was in the particles $>8\mu$m, low in the 1 - 8μm particles and only a few percent in 0.4 - 1μm particles. It was shown in these studies that the efficiency of atom formation in the plasma form the elements in the particulate

matter depends on the size of the particles. The particle size also influences the efficiency of nebulization in the ICP system.

3. References

2.1 Finotello, F., Analytical methods for the Liberty spectrometer

2.2 Ebdon, L., and Cave, M.R., Analyst, 1982, **106**, 172

2.3 Olson, K.W., Haas, W.J.Jr., and Fassel, V.A., Anal. Chem., 1977, **49**, 632

2.4 Scott, R.H., Fassel, V.A., Kniseley, R.N., and Nixan, D.E., Anal. Chem., 1974, **46**, 75

2.5 Fassel, V.A., and Kniseley, R.N., Anal. Chem., 1974, **46**, 1155A

2.6 Moore, G.L., Introduction to Inductively Coupled plasma Atomic Emission Spectrometry

2.7 Reed, T.B., J. Appl. Phys., 1961, 32, **821**, 2534

2.8 Fassel, V.A.,"Electrical Plasma Spectroscopy" XVI Colloquium Spectroscopicum Internationale, Adam Hilger, london, 1973

2.9 Fassel,V.A., and Kneseley, R.N., Anal. Chem., 1974, **46**, 1155A

2.10 Koirtyohann, S.R., Jones, J.S., and Yates, D.A., Anal. Chem., 1980, **52**, 1965

2.11 Olesik, J.W., Anal. Chem., 1991, **63**, 12A

2.12 Boumans, P.W.J.M., Vrakking, J.J.A.M., Spectrochim. Acta, 1987,**42B**, 819

2.13 Wohler, C.C., ICP Information Newsletter, 1985, **10**, 601

2.14 Ramsey, M., and Thompson, M., J Anal. At. Spectrom., 1986, **1**, 185

2.15 Olesik, J.W., and Moore, A.W.Jr, Anal. Chem., 1990, **62**, 840

2.16 Botto, R.I., Spectrochim. Acta, 1985, **40B**, 397

2.17 Farino, J., Miller, J.R., Smith, D.D., and Browner, R.F., Anal. Chem., 1987, **59**, 2303

2.18 Faires, L.M., and Niemczyk, T.M, Appl. Spectrosc.,1983, **37**, 553

2.19 Tripkovic, M.R., and Holclajtner-Antunovic, I.D., J. Anal. At. Spectrom., 1993, **8**, 349

2.20 Hettipathirama, T.D., Wade, A.P., and Blade,M.W., Spectrochim. Acta,

2.21 Basseh, J., Denny, R.C., Jeffery, G.H., and Mendham, J., Vogel's textbook of quantitative inorganic analysis, 1978, 4th edn, 8, London

2.22 Thompson, M., and Ramsey, M.H., Analyst, 1985, **110**, 1413

2.23 Gunter, W., Visser, K., and Zeeman, P.B., Spectrochim. Acta, 1985, **40B**, 617

2.24 Koirtyohan, S.R., Jones, J.S., Jester, C.P., and Yates, D.A., Spectrochim. Acta, 1981, **36B**, 49

2.25 Canals, A., Wagner, J., and Brower, F., Spectrochim. Acta, 1988, **43B**, 1321

2.26 Prell, L.J., Mornig, C., Harries, R.E., and Koirtyohann, S.R., Spectrochim. Acta, 1989, **40B**, 1401

2.27 Abdallah, M.H., Mermet, J.M., and Tracy, C., Anal. Chim. Acta, 1976, **87**, 329

2.28 Caughlin, B.L, and Blades, M.W.,Spectrochim. Acta, 1985, **40B**, 987

2.29 Hanselman, D.S., Sesi, N.N., Huang, M., and Hieftjie, G.M., Spectrochim. Acta, 1994, **49B**, 495

2.30 Low, G.K.C., Batley, G.E., and Buchanan, S.J., Anal. Chim. Acta, 1987, **197**, 327

2.31 Omenetto, N., Spectrochim Acta., 1988, **42B**, 63

2.32 Wu, M., and Hieftjie, G.M., Spectrochim. Acta, 1994, **49B**, 149

2.33 Blades, M.W., and Horlick, G., Spectrochim. Acta, 1981, **36B**, 881

2.34 Mermet, J.M., and Robin, J., Anal. Chim. Acta, 1975, **70**, 271

2.35 Kalnicky, D.J., Fassel, V.A., and Kniseley, R.N., Appl. Spectrosc., 1977, **31**, 139

2.36 Boumans, P.W.J.M., and DeBoer, F.J., Spectrochim. Acta, 1976, **31B**, 355

2.37 Howatson, M., Introduction to gas discharge, Pergamon Press, Oxford, 1976

2.38 Murayama, S., Matsumo, H., and Yamamoto, M., Spectrochim. Acta., 1968, **23B**, 513

2.39 Murayama, S., Spectrochim. Acta, 1970, **25B**, 191

2.40 Kornblum, G.R., and Degalan, L., Spectrochim. Acta, 1977, **32B**, 455

2.41 Larson, G.F., Fassel, V.A., Scott, R.H., and Knisely, R.N., Anal. Chem., 1975, **47**, 238

2.42 Olesik, J.W., and Williamsen, E.J., Appl. Spectrosc., 1989, **43**, 1223

2.43 Mermet, J.M., Anal. Chim. Acta, 1991, **250**, 85

2.44 Li, K.P., Hwang, J.D., and Winerfordner, J.D., Anal. Chem., 1990, **62**,1233

2.45 Veillon, C., and Margoshes, M., Spectrochim. Acta, 1968, **23B**, 503

2.46 Franklin, M., Baber, C., and Koirtyohan, S.R., Spectrochim. Acta, 1976, **31B**, 489

2.47 Paama, L., and Piiri, L., J. Anal. At. Spectrom., 1995, **10**, 117

2.48 Gladney, E.S., and Roelandts, I., Geostand. Newl., 1990, **14**, 21

2.49 Ambe, Y., and Nishikawa, M., Anal. Chim. Acta, 1987, **193**, 355

2.50 Winge, R.K., Fassel, V.A., Peterson, V.J., and Floyd, M.A., Inductively-Coupled Plasma Atomic Emission Spectrometry, 1985, **548**, Elsevier, Amsterdam

CHAPTER 3: PHYSICAL INTERFERENCES BY MINERAL ACID IN ICP-OES

3.1 INTRODUCTION

Mineral acids are commonly used for sample preparation, eg. extraction, digestion or dissolution and consequently are major components of the sample matrix. Several methods are used for compensating for the effects of acids interferences during an analysis. The most successful and most commonly used approaches involve matrix matched calibration standards and standard addition method[1]. Internal standardization has also been used to improve the performance of ICP-OES by (indirectly) reducing plasma noise[2] and matrix interferences. Several methods may be used to remove the interfering species eg. chemical separation. Solution uptake is of considerable practical importance as concentrated acids have an effect on the emission signal of the analyte in ICP-OES.

In ICP emission spectral analysis, special attention is paid to physical interferences where transport aerosol effects can affect the line intensity[3]. Greenfield *et al*[4] reported that signal reductions resulting from high acid concentrations were direct result of reduced analyte transport to the plasma. For reducing the transport aerosol effects in the analysis of materials the internal standard method has only been used[2,5]. However, it has been discussed that its use in routine work can lead to a reduction of accuracy if the internal standard and the analyte have no close atomic transition[6]. The effects

of mineral acid physical interferences on the determination of iron in acidic media in ICP-OES is described in this study.

3.2 EXPERIMENTAL

3.2.1 Instrumentation

A Spectroflame ICP manufactured by Spectro-Analytical instrument was employed for all measurements. The instrument is fitted with vacuum and air polychromator and Sequential monochromator covering the region 200 to 480nm. The excitation source was an Ar plasma. The plasma conditions used throughout, unless otherwise stated, are given in table 1. The sample introduction system consisted of a cross-flow nebulizer and associated double-pass spray chamber. Samples were introduced into the nebulizer by means of a peristaltic pump. An integration time of 1s was employed for all measurements. Precision data were obtained for five integrations.

3.2.2 Reagents

All reagents used were of analytical-reagent grade (AR). Standard solutions were prepared from stock solution containing 1000μg/ml of Fe supplied by Merck. Working standards were freshly prepared by dilution of the stock solution with de-ionised water. Matrix solutions of HNO_3, HCl and H_2SO_4 were prepared from available AR

acids. High purity Spec. grade Ar was used as the plasma and nebulization gas.

3.2.3 Table 1 Plasma parameters

Carrier gas flow-rate [l/min^{-1}]	0.65
Auxiliary gas flow-rate [l/min^{-1}]	0.70
Plasma gas flow-rate [l/min^{-1}]	0.90
Applied power [kW]	1.30

3.2.4 Procedure

3.2.4.1 Investigation of [HCl], [HNO_3] and [H_2SO_4] interferences on Fe

A number of solutions containing 1; 5; 10; 20 and 50μg/ml of Fe in solutions containing 0-50%(v/v) HNO_3; HCl and H_2SO_4 were prepared. The influence of the concentrations of these acids on Fe were determined by measuring the emission intensity of the analyte at different concentrations. Three analytical lines were chosen viz. Fe II 238.20nm, Fe II 239.56nm and Fe II 259.94nm. Background correction was

employed for all emission signal. In this procedure, the normal calibration method was employed for all analysis. The results were presented as %acid(v/v) in Fe against the emission intensity.

3.2.4.2 Investigation of sample transport efficiency of Fe in different concentrations of H_2SO_4, HCl and HNO_3

The sample transport efficiency of Fe in 0-50%(v/v) of the acids from the peristaltic pump to the plasma was investigated. It was defined as the amount of aerolsol which have reached the plasma per time unit. The amount of aerosol which have reached the plasma was determined for each concentration of the acid by determining the amount of solution aspirated per time unit as well as by collecting the amount of aerosol gone to waste per time unit.

The acid aerosol delivered to the nebulizertip with the aid of the peristaltic pump was recorded for each concentration. The amount of acid aerosols wasted in the double-pass spray chamber per time unit were collected in a U-shaped tube. The spray chamber was then rinsed with 20ml of de-ionized water to wash out the remaining acid. These aerosols (5 replicates) were transferred into 50ml volumetric flasks. Three drops of phenolphthlalein indicator were added to each flask. They were then titrated with standardized solutions of sodium hydroxide (NaOH). The avarage volume of NaOH obtained at the endpoint was then used to calculate the amount of wasted acid

aerosols. The total volume of the aerosol reaching the plasma per time unit is therefore the difference between the amount delivered by the pump and the amount wasted per time unit.

3.3 RESULTS AND DISCUSSION

3.3.1 Effects of the different concentrations of the acids on the emission signal of Fe

Figure 5 - 13 shows the effect of HNO_3, HCl and H_2SO_4 on the emission intensity of the Fe II 259.94nm, Fe II 238.20nm and Fe II 239.56nm lines respectively. From the results in the figures, it can be seen that HNO_3 and HCl enhance the emission intensity of Fe at low levels. HNO_3 and HCl enhance (1; 5 and 10μg/ml) and 1μg/ml respectively. The amount of enhancement decreases as the concentration of these acids increases. HNO_3 depresses the emission signal of Fe at 20 and 50μg/ml whereas HCl depresses the emission signal of Fe at 5; 10; 20 and 50μg/ml. H_2SO_4 depresses the emission intensity of Fe at all levels.

Table 2 shows the analyte signal recoveries of Fe in HNO_3, HCl and H_2SO_4 respectively. The analyte signal recovery of 50μg/ml Fe II 259.94nm are reduced to 85%; 89% and 38% by the presence of 50%(v/v) HNO_3; HCl and H_2SO_4 respectively (where the signal recovery was calculated as percentage of the response obtained for

aqueous analyte solution). It can be concluded that the presence of an acid in a sample either enhances or depresses the emission signal of an analyte. The amount of enhancement or depression depends on the concentration of both the analyte and the acid used. Results obtained for the 238.20 and 239.56nm lines were almost similar to that of Fe II 259.94nm.

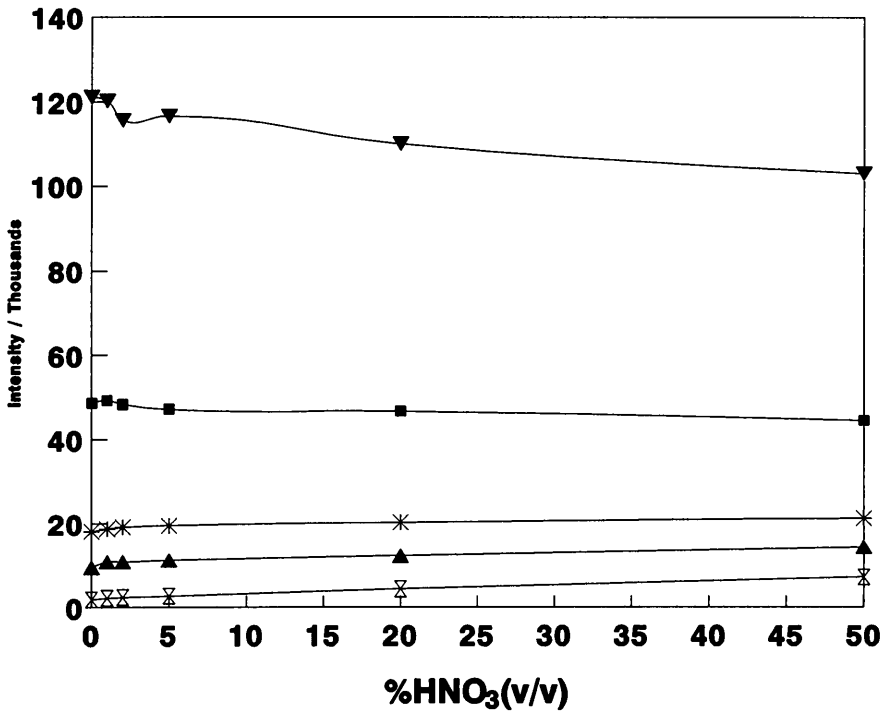

Figure 5. Effect of the concentration of HNO_3 on the emission intensity of Fe II 259.94nm. ⧖ 1μg/ml; ▲ 5μg/ml; ∗ 10μg/ml; ■ 20μg/ml; ▼ 50μg/ml

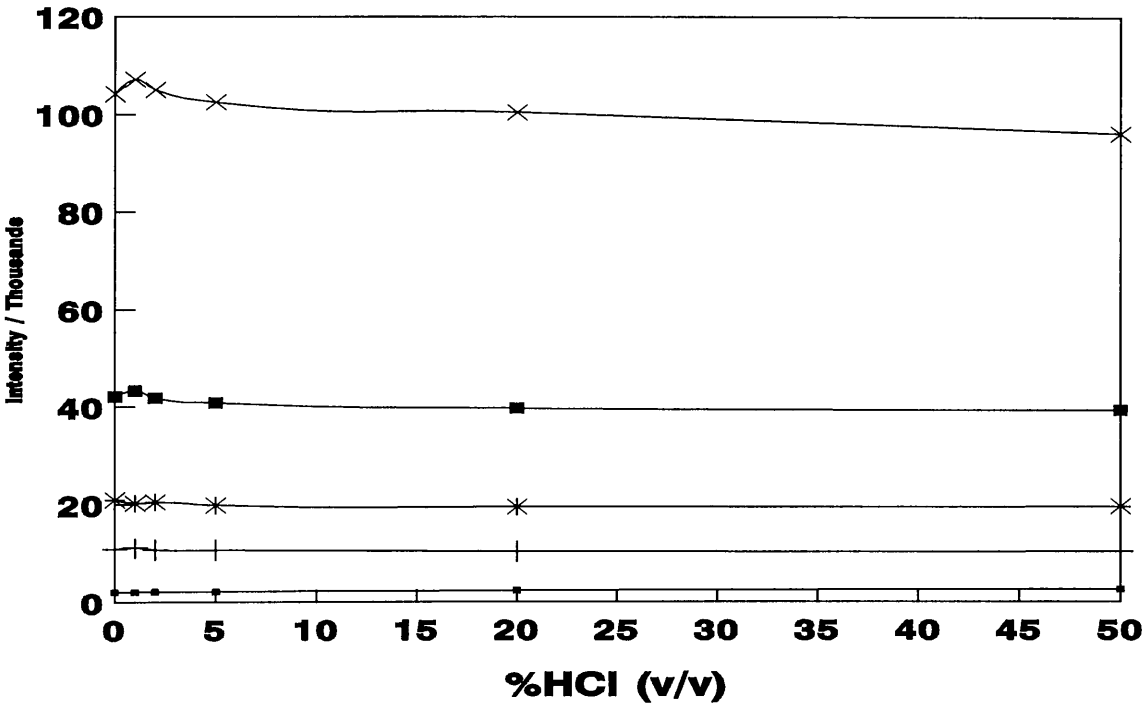

Figure 6. Effects of the concentration of HCl on the emission intensity of Fe II 259.94nm. ▪ 1μg/ml; + 5μg/ml; ∗ 10μg/ml; ■ 20μg/ml; × 50μg/ml

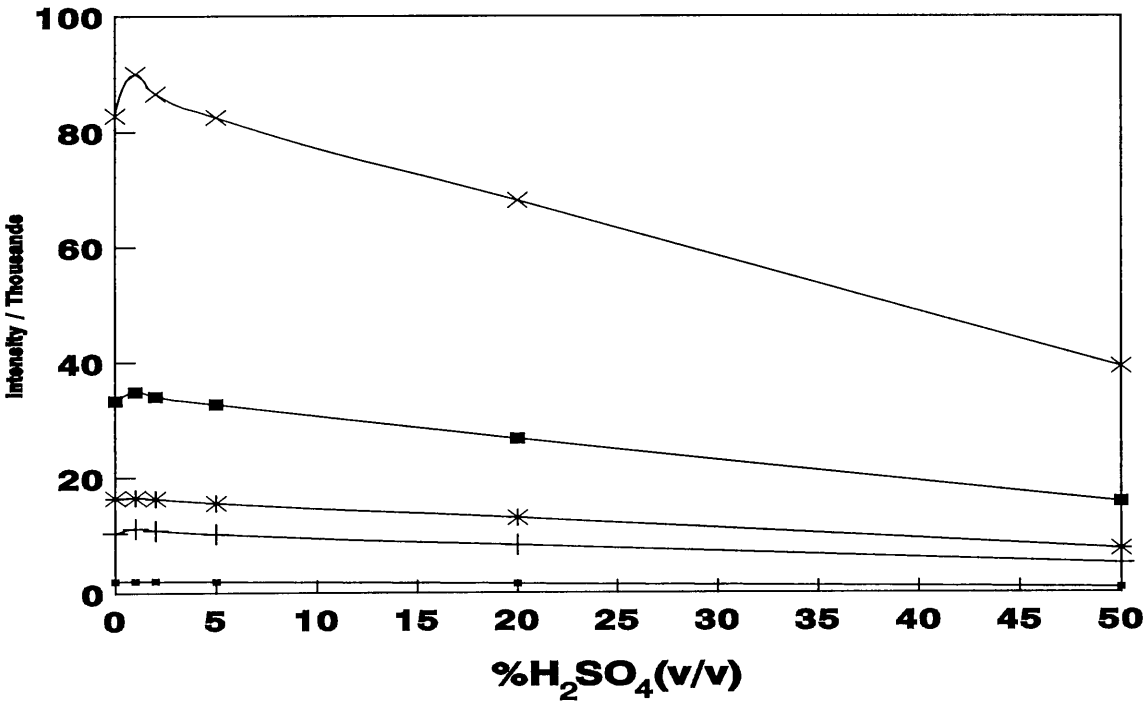

Figure 7. Effect of the concentration of H_2SO_4 on the emission signal of Fe II 259.94nm. ▪ 1μg/ml; + 5μg/ml; ∗ 10μg/ml; ■ 20μg/ml; × 50μg/ml

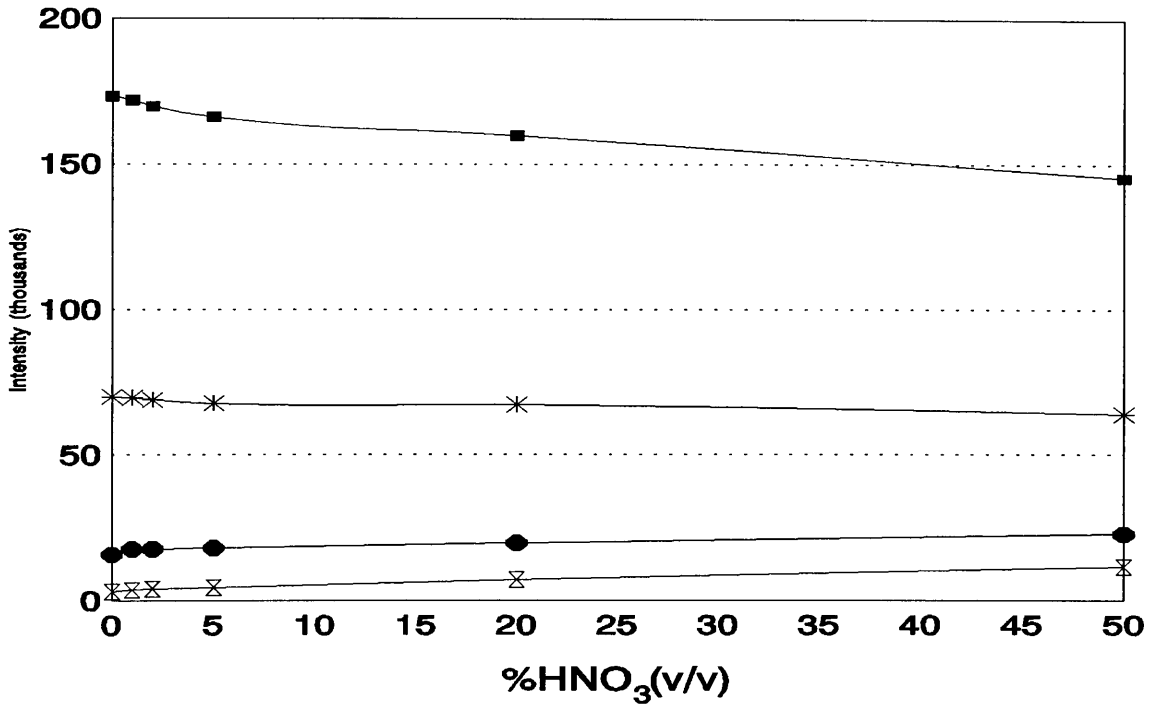

Figure 8. Effect of the concentration of HNO_3 on the emission intensity of Fe II 238.20nm. ⧖ 1μg/ml; ● 5μg/ml; ∗ 20μg/ml; ■ 50μg/ml

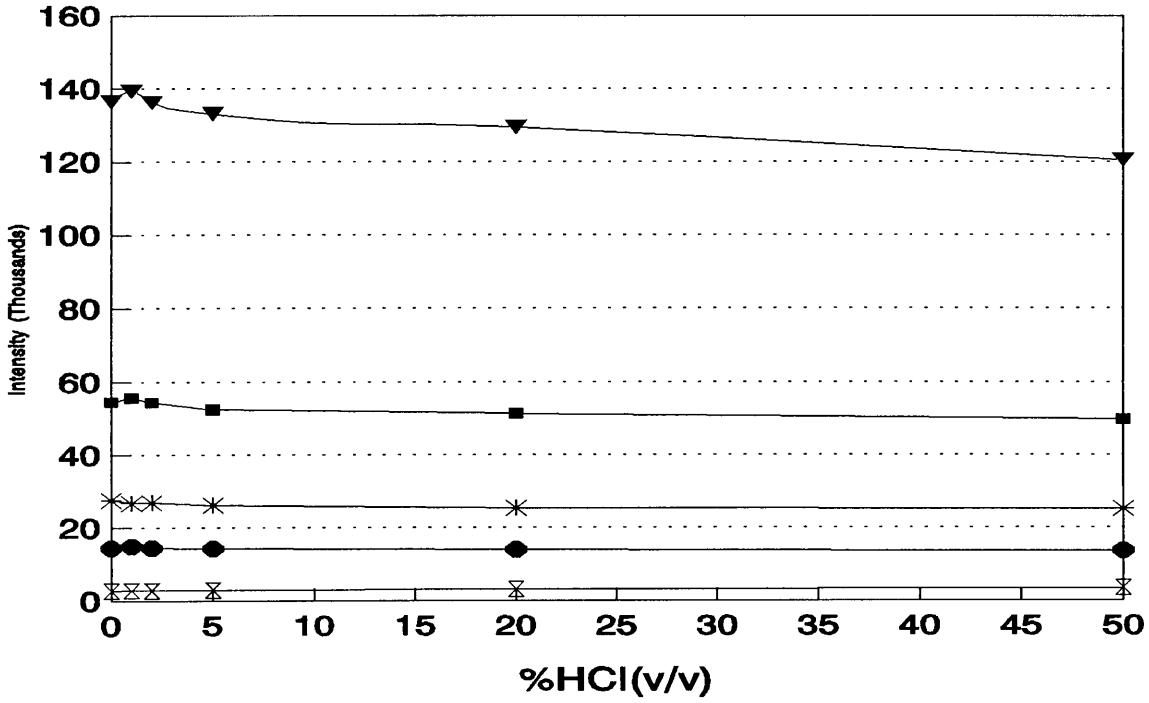

Figure 9. Effect of the concentration of HCl on the emission signal of Fe II 238.20nm. ⧖ 1μg/ml; ● 5μg/ml; ∗ 10μg/ml; ■ 20μg/ml; ▾ 50μg/ml

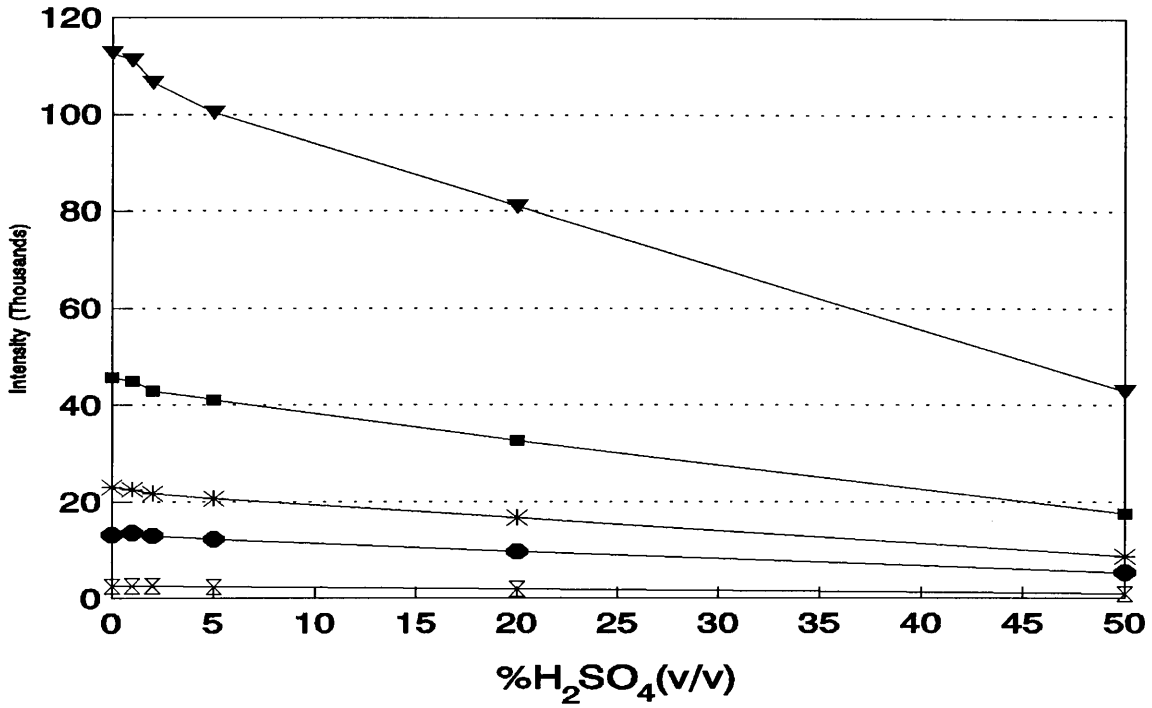

Figure 10. Effect of the concentration of H_2SO_4 on the emission signal of Fe II 238.20nm. ⧖ 1μg/ml; ● 5μg/ml; ∗ 10μg/ml; ■20μg/ml; ▼ 50μg/ml

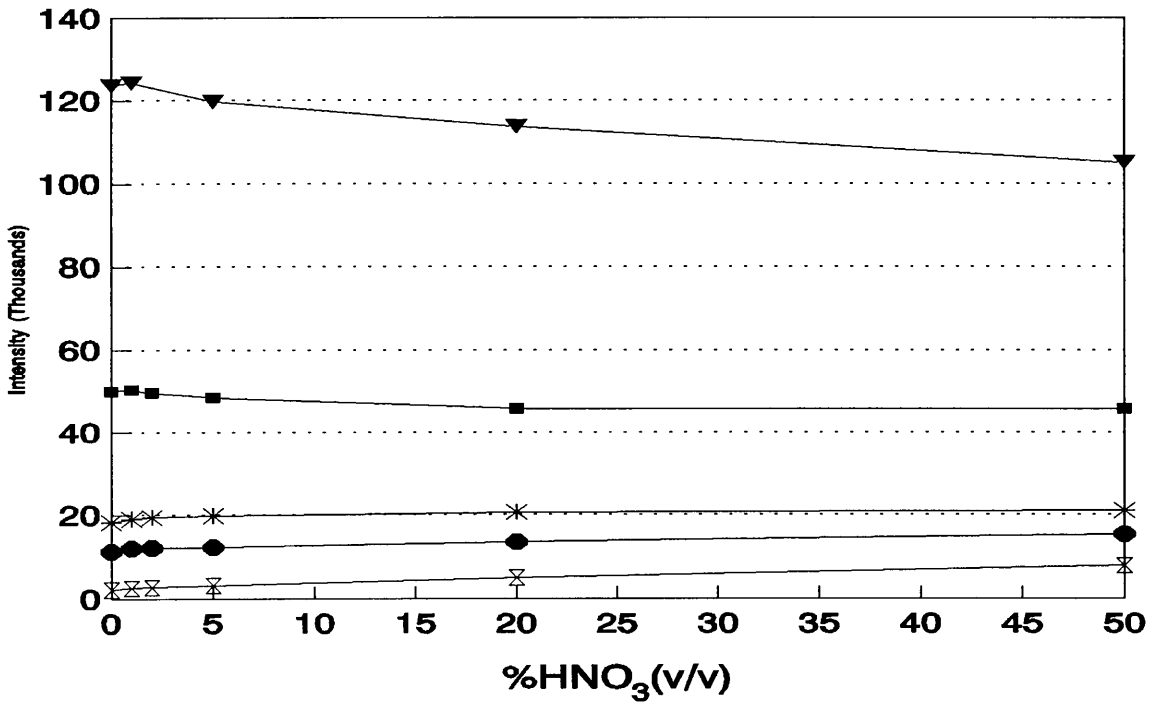

Figure 11. Effect of the concentration of HNO_3 on the emission signal of Fe II 239.56nm. ⧖ 1μg/ml; ● 5μg/ml; ∗ 10μg/ml; ■ 20μg/ml; ▼ 50μg/ml

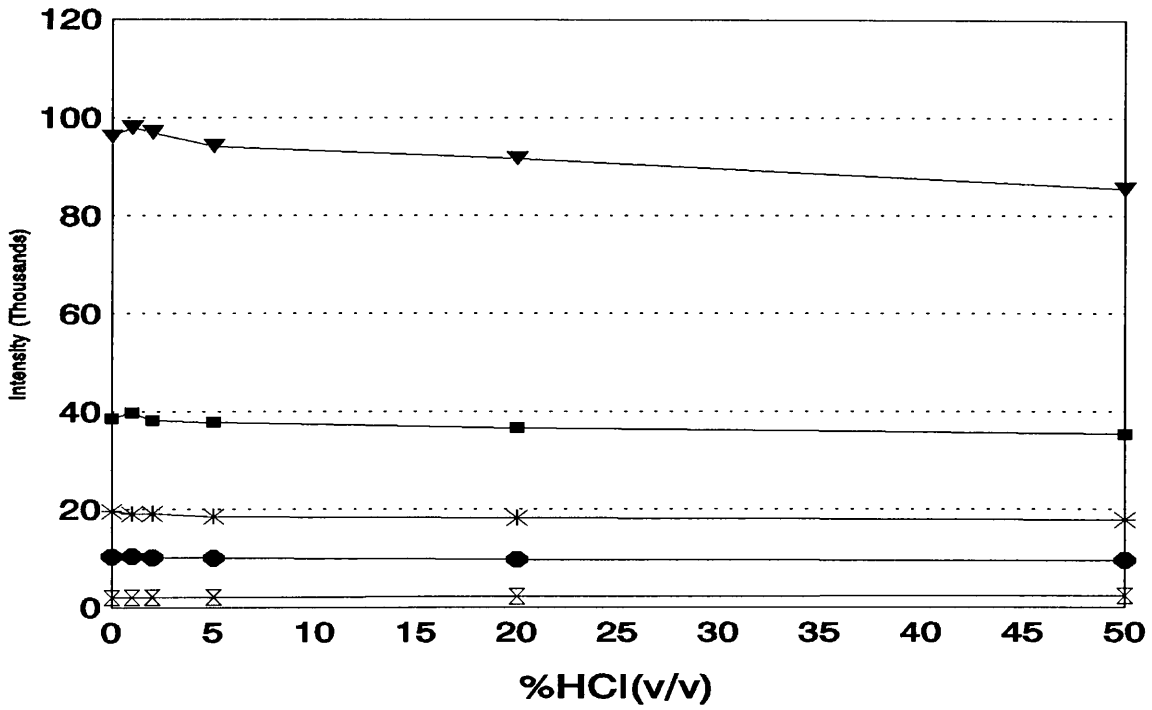

Figure 12. Effect of the concentration of HCl on the emission signal of Fe II 239.56nm. ⧖ 1μg/ml; ● 5μg/ml; ∗ 10μg/ml; ■ 20μg/ml; ▼ 50μg/ml

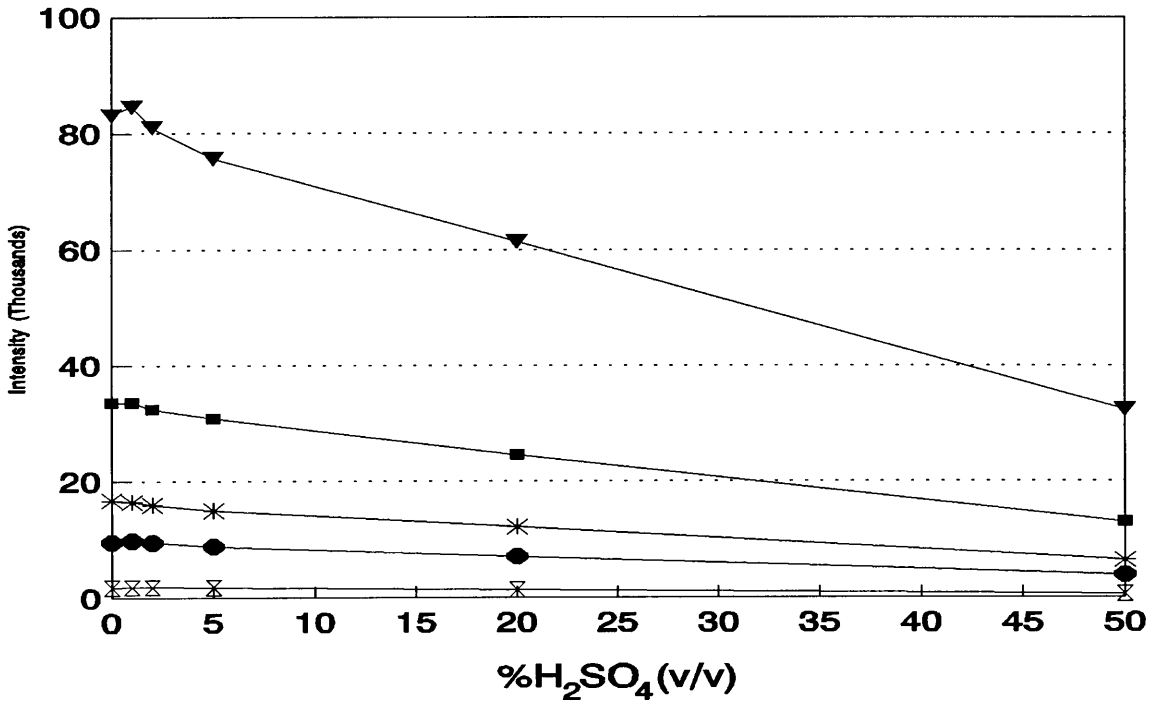

Figure 13. Effect of the concentration of H_2SO_4 on the emission signal of Fe II 239.56nm. ⧖ 1μg/ml, ● 5μg/ml; ∗ 10μg/ml; ■ 20μg/ml; ▼ 50μg/ml

Table 2: Effect of HNO_3, HCl and H_2SO_4 on the recovery of Fe

Fe Concentration [μg/ml]		%Recovery														
		HNO_3					HCl					H_2SO_4				
		A	B	C	D	E	A	B	C	D	E	A	B	C	D	E
1	FeII 238.20nm	120	128	143	229	369	101	101	105	111	121	102	102	95	76	37
	FeII 239.56nm	117	125	142	225	356	102	103	104	107	118	104	104	99	76	34
	FeII 259.94nm	121	128	146	235	386	103	104	104	112	125	102	102	95	76	37
5	FeII 238.20nm	112	113	114	125	144	103	100	99	96	94	103	99	93	73	41
	FeII 239.56nm	107	108	109	120	136	101	98	97	94	92	103	100	92	74	40
	FeII 259.94nm	114	114	117	129	150	103	99	98	95	95	106	104	98	80	48
10	FeII 238.20nm	101	104	105	109	112	97	98	95	92	91	98	94	90	72	38
	FeII 239.56nm	104	107	108	113	116	97	98	95	93	91	98	95	89	72	38
	FeII 259.94nm	103	106	108	112	118	97	98	95	93	93	101	99	95	79	46
20	FeII 238.20nm	100	99	97	96	91	102	100	96	94	91	98	94	90	72	38
	FeII 239.56nm	101	99	97	97	92	103	99	98	95	92	100	97	92	73	39
8	FeII 259.94nm	101	99	97	96	91	102	99	98	94	93	105	102	98	80	47
8	FeII 238.20nm	99	98	96	92	84	102	100	98	95	88	99	95	89	72	38
50	FeII 239.56nm	101	97	97	92	85	103	101	98	95	89	102	97	91	74	39
	FeII 259.94nm	99	95	96	91	85	103	101	98	96	92	108	104	99	82	47

A ≡ 1%(v/v)
B ≡ 2%(v/v)
C ≡ 5%(v/v)
D ≡ 20%(v/v)
E ≡ 50%(v/v)

3.3.2 Variation of the peristaltic pump speed to determine the rate at which different concentrations of H_2SO_4 should be pumped so that equal volumes are transported to the nebulizertip

As H_2SO_4 has higher density and lower viscosity than HNO_3 and HCl, it was necessary to determine the effect of solvent transport efficiency of different concentrations of this acid. This was achieved by using a peristaltic pump with adjustable speed. The main aim of this was to determine the compromise pump speed for each concentration so that equal volumes of different concentration of this acid can be delivered to the nebulizertip. A calibration curve was then drawn whereby volume of H_2SO_4 delivered by the pump per minute was plotted against pump speed.

Table 3: The density of concentration of the acid

$\%H_2SO_4$(v/v)	density/g
0	1.0000
1	1.0109
2	1.0201
5	1.0573
10	1.1093
20	1.2056
30	1.3111
50	1.4877

Table 4: The amount of aerosol delivered to the nebulizer tip per minute

	Amount of H_2SO_4 delivered per minute/g							
Speed / rpm	0%(v/v) H_2SO_4	1%(v/v) H_2SO_4	2%(v/v) H_2SO_4	5%(v/v) H_2SO_4	10%(v/v) H_2SO_4	20%(v/v) H_2SO_4	30%(v/v) H_2SO_4	50(v/v) %H_2SO_4
200	0.3215	0.3260	0.3314	0.3458	0.3688	0.4021	0.4356	0.4969
400	0.6668	0.6748	0.6819	0.6927	0.7395	0.8105	0.8727	0.9844
600	0.9864	1.0007	1.0176	1.0511	1.1078	1.2161	1.3064	1.4758
800	1.3488	1.3725	1.3866	1.4155	1.4982	1.5854	1.7164	1.9252
900	1.5497	1.5627	1.5829	1.6280	1.7180	1.8536	1.9838	2.1965

Table 5: The amount of aerosols delivered to the nebulizertip per minute

	Amount of H_2SO_4 delivered per minute/ml							
Speed / rpm	0%(v/v) H_2SO_4	1%(v/v) H_2SO_4	2%(v/v) H_2SO_4	5%(v/v) H_2SO_4	10%(v/v) H_2SO_4	20%(v/v) H_2SO_4	30%(v/v) H_2SO_4	50(v/v) $\%H_2SO_4$
200	0.3215	0.3225	0.3278	0.3271	0.3325	0.3335	0.3322	0.3340
400	0.6668	0.6675	0.6746	0.6552	0.6666	0.6723	0.6658	0.6617
600	0.9864	0.9899	1.0066	0.9941	0.9987	1.0087	0.9964	0.9920
800	1.3488	1.3577	1.3717	1.4155	1.3506	1.3150	1.3091	1.2941
900	1.5497	1.5459	1.5658	1.5400	1.5487	1.5375	1.5131	1.4764

From the calibration curve, see figure 14, a plot of volume of H_2SO_4 delivered by the peristaltic pump per minute against speed, it was shown that the change in the flow-rate of the acid is minimum. It can therefore be concluded that the slight decrease in the amount of aerosols delivered to the nebulizertip is not contributing to the depressant effect of the analyte emission signal as $\%H_2SO_4$(v/v) increases.

3.3.3 Effects of acids on the solvent transport efficiency

Figure 15 shows the amount of HNO_3, HCl and H_2SO_4 aerosol delivered by the pump to the nebulizer tip for different concentrations of these acids. Figure 16 and 17 shows the sample transport efficiency as the amount of HNO_3 and HCl aerosol reaching the plasma per time unit respectively for different concentration of the acids. The total volume of the aerosol reaching the plasma per time unit is the difference between the amount delivered by the pump and the amount wasted per time unit. The decrease in the sample mass transport of HNO_3 and H_2SO_4 to the nebulizer tip may be caused by the decrease in viscosity as their concentration increases. Farino *et al*[7] also reported a decrease in sample mass transport of H_2SO_4 as its concentration increases. There is no significant change in the amount of HCl delivered by the pump at different acid concentrations. The sample transport efficiency of HNO_3 and HCl is unaffected by the changes of mass transport to the nebulizer tip as the amount of aerosol reaching the plasma are almost the same for all concentrations.

Table 6: The determination of the amount of aerosol delivered to both the nebulizer tip and the plasma for different concentration of H_2SO_4

$\%H_2SO_4$	$[H_2SO_4]$ mol/dm^3	density/ g	V_x		[NaOH] mol/dm^3	Average NaOH titrated/ml	V_y (ml/min)	$V_x - V_y$ (ml/min)
			g/min	ml/min				
0	0.0000	0.0000	1.6830	1.6830	-	-	-	-
1	0.1876	1.0160	1.6960	1.6693	0.0750	8.2	1.6291	0.0402
2	0.3752	1.0276	1.7012	1.6555	0.1450	8.3	1.6038	0.0517
5	0.9380	1.0584	1.7464	1.6500	0.3625	7.4	1.5458	0.1042
10	1.8760	1.1133	1.8323	1.6458	0.7350	7.3	1.4300	0.2158
20	3.7520	1.2138	1.9930	1.6420	1.4200	7.5	1.4192	0.2228
30	5.6281	1.3060	2.1246	1.6268	2.2000	7.1	1.3877	0.2391
50	9.3801	1.4859	2.3793	1.6013	3.6250	7.0	1.3526	0.2487

$V_x \equiv$ The volume of H_2SO_4 delivered by the pump per minute

$V_y \equiv$ Average H_2SO_4 wasted per minute

$V_x - V_y \equiv$ Amount of H_2SO_4 aerosols leading to the plasma

Table 7: The determination of the amount of aerosol delivered to both the nebulizer tip and the plasma for different concentration of HNO_3

$\%HNO_3$(v/v)	$[HNO_3]$ mol/dm^3	density/ g	V_x		[NaOH] mol/dm^3	Average NaOH titrated/ml	V_y ml/min	$V_x - V_y$ (ml/min)
			g/min	ml/min				
0	0.0000	1.0000	1.8643	1.8643	-	-	-	-
1	0.1465	1.0042	1.8659	1.8581	0.0300	8.7	1.7877	0.0704
2	0.2930	1.0084	1.8720	1.8564	0.0550	9.4	1.7683	0.0881
5	0.7325	1.0210	1.8830	1.8443	0.1450	8.8	1.7380	0.1063
10	1.4651	1.0546	1.9275	1.8277	0.2957	8.8	1.7741	0.0536
20	2.9302	1.1007	2.0037	1.8204	0.5667	8.9	1.7271	0.0933
30	4.3952	1.1472	2.0852	1.8176	0.8533	8.8	1.7124	0.1052
50	7.3254	1.2338	2.2375	1.8135	1.4167	8.9	1.7270	0.0865

$V_x \equiv$ The volume of HNO_3 delivered by the pump per minute

$V_y \equiv$ Average HNO_3 wasted per minute

$V_x - V_y \equiv$ Amount of HNO_3 aerosols leading to the plasma

Table 8: The determination of the amount of aerosol delivered to both the nebulizer tip and the plasma for different concentration of HCl

%HCl(v/v)	[HCl] mol/dm^3	density/ g	V_x		[NaOH] mol/dm^3	Average NaOH titrated/ml	V_y ml/min	$V_x - V_y$ (ml/min)
			g/min	ml/min				
0	0.0000	1.0000	1.8428	1.8428	-	-	-	-
1	0.1208	1.0019	1.8525	1.8490	0.0300	6.9	1.7136	0.1354
2	0.2415	1.0038	1.8562	1.8484	0.0550	7.7	1.7536	0.0948
5	0.6038	1.0095	1.8640	1.8464	0.1450	7.2	1.7170	0.1294
10	1.2076	1.0190	1.8850	1.8499	0.2957	7.0	1.7141	0.1358
20	2.4153	1.0380	1.9204	1.8500	0.5667	7.4	1.7363	0.1137
30	3.6229	1.0570	1.9612	1.8479	0.8533	7.3	1.7194	0.1285
50	6.0382	1.0950	2.0226	1.8471	1.4167	7.4	1.7362	0.1109

$V_x \equiv$ The volume of HCl delivered by the pump per minute

$V_y \equiv$ Average HCl wasted per minute

$V_x - V_y \equiv$ Amount of HCl aerosols leading to the plasma

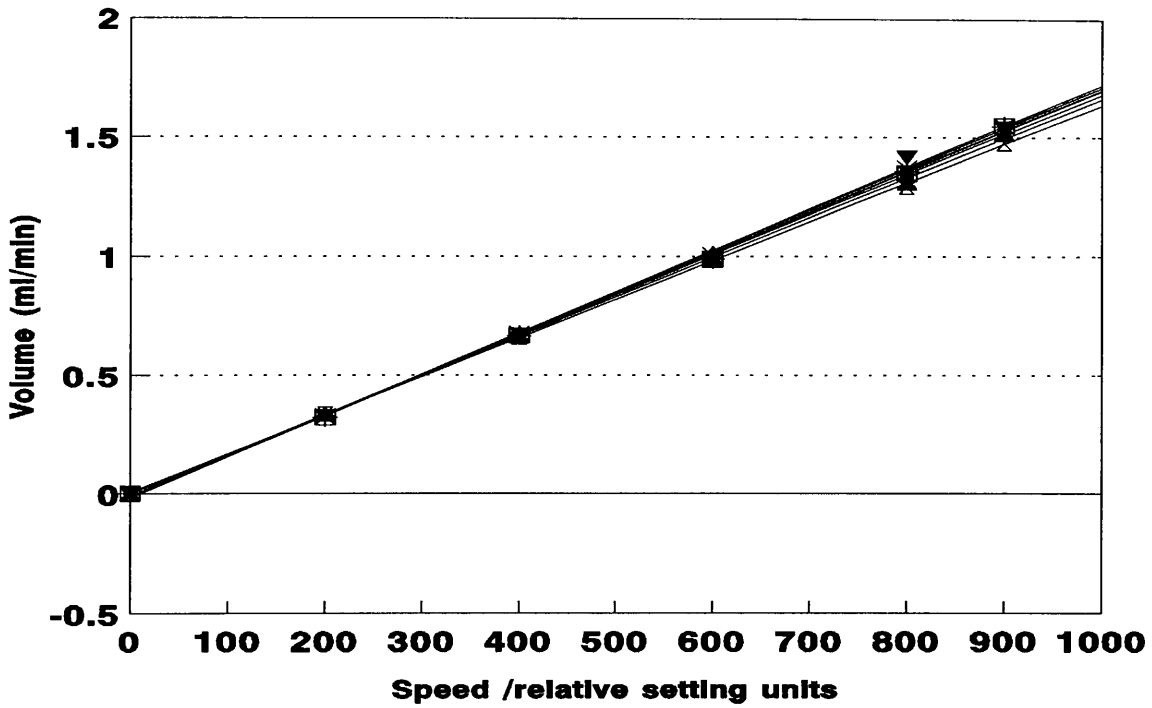

Figure 14. The volume of H_2SO_4 delivered by the pump at different speed. □ 0%; + 1%; ∗ 2%; ▾ 5%; ■ 10%; ♦ 20%; ▲ 30% and ⧖ 50% H_2SO_4

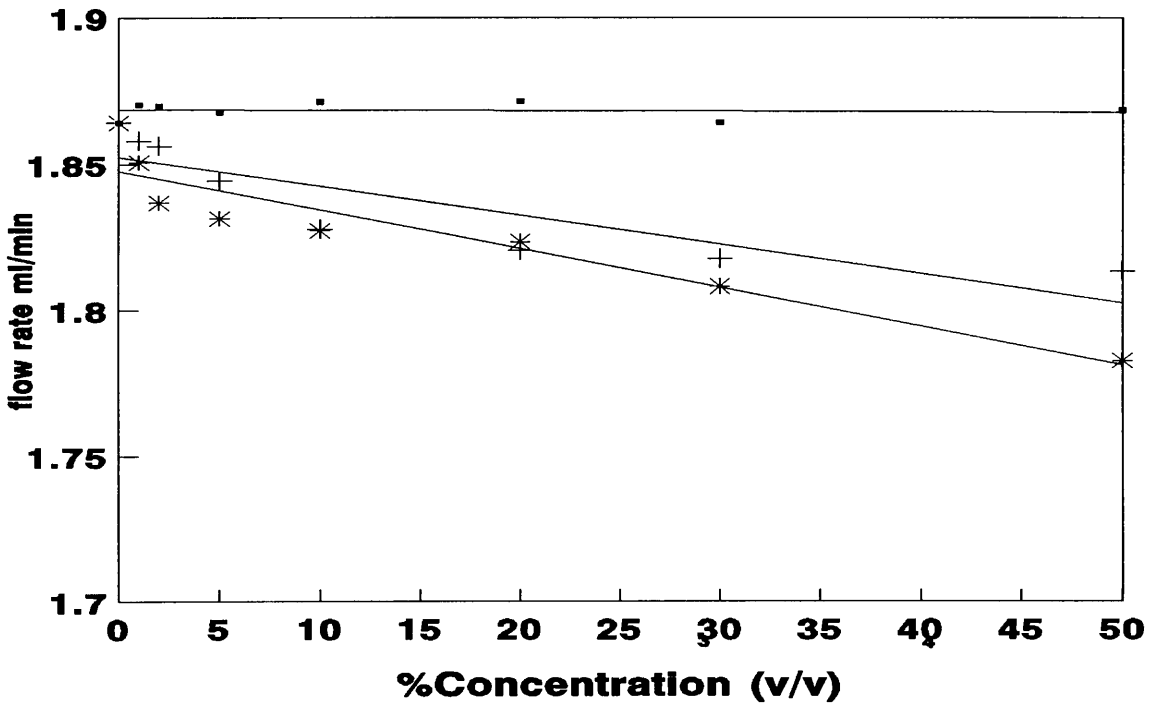

Figure 15. The amount of HNO_3, HCl and H_2SO_4 aerosols delivered by the pump to the nebulizer tip for different concentration of these acids

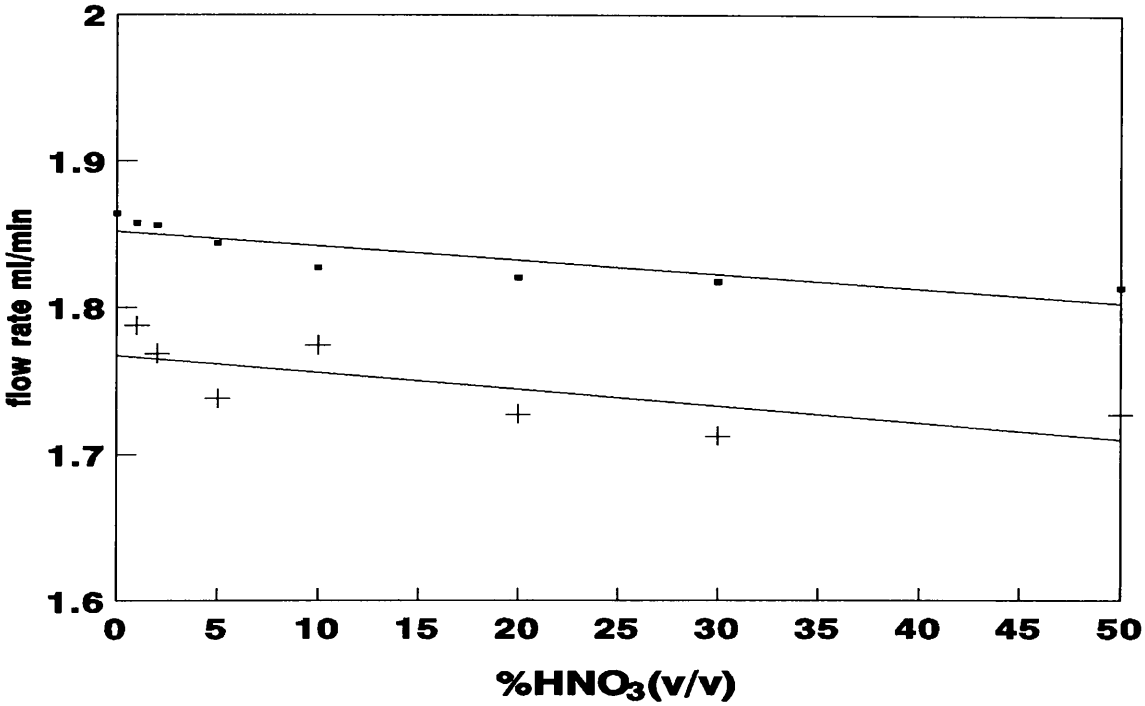

Figure 16. The amount of HNO_3 aerosol delivered to the plasma per time unit for different concentration of this acid. ▪ Amount deliverd; + Amount wasted

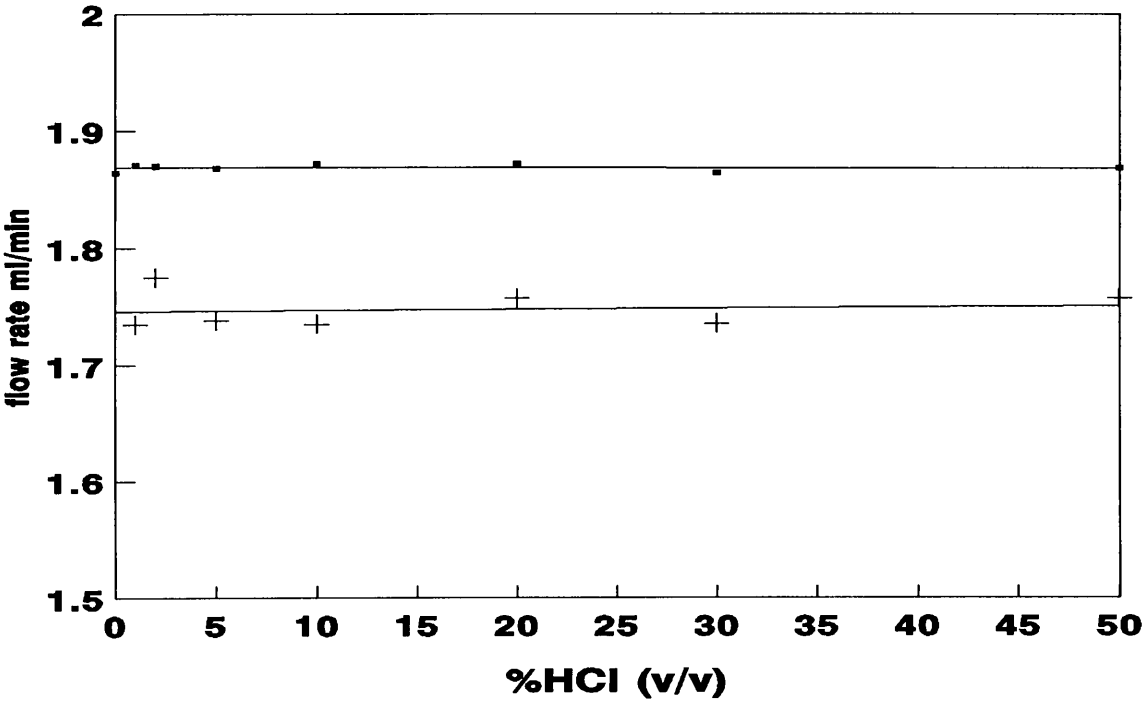

Figure 17. The amount of HCl aerosol deliverd to the plasma per time unit for different concentration of this acid. ▪ Aerosol delivered; + Aerosol wasted

3.4 Conclusion

It can be concluded that the emission signal of Fe depends on the concentration and the properties of the mineral acid used as well as the operating conditions of the plasma. It was also found in determining the sample transport efficiency that the acid interferences of Fe in ICP-OES are not caused by the decrease or increase in the amount of aerosol reaching the plasma. The magnitude of these effects, however, is affected by various factors in a complicated way which needs further investigation.

3.5 References

3.1 Kalivas, J.H., and Kowalski, B.R., Anal. Chem., 1982, **54**, 560

3.2 Schmidt, G.J., and Slavin, W., Anal. Chem., 1982, **54**, 2491

3.3 Maessen, F.J.M.J., Balke, J., and de Boer, J.L.M., Spectrochim. Acta, 1982, **37B**, 517

3.4 Greenfield, S., McGeachim, H., and Smith, P.B., Anal. Chem., 1976, **84**, 67

3.5 Zadgorska, Z., Nikel, H., Mazurkiewicz, M., and Wolf, G., Fresenius Z Anal. Chem., 1983, **314**, 356

3.6 Salin, E., and Horlick, G., Anal. Chem., 1980, **52**, 1578

3.7 Farino, J., Miller, J.R., Smith, D.D., and Browner, R.F., Anal. Chem., 1987, **59**, 2303

CHAPTER 4: ANALYSIS OF ZIRCONIUM OXIDE (ZrO_2)

4.1 Dissolution of ZrO_2

Sample preparation, the conversion of the raw sample material into a form suitable for presentation to an instrument, is often regarded as the "Achilles Heel" of atomic spectrometry, a time-consuming and messy ordeal that has to be endured before the analyst can get down to the real business of instrumental analysis[1]. For this reason there has been increasing interest and a moderate degree of success in the direct use of solid samples with no prior chemical preparation. It seems unreasonable to assume that chemical decomposition will be avoidable even when solid introduction methods are eventually perfected. To achieve better selectivity, chemical separation will still be required, a recourse not associated with solid-sampling techniques. Thus there is a need of achieving such rapid methods of separation, especially in low trace analysis, an area where interference is often the main limiting factor.

The refractory character of ZrO_2 and its high chemical resistance renders its sample pretreatment difficult, and accordingly its decomposition needs highly aggressive reagents. To bring ZrO_2 into solution, pressure decomposition in PTFE bombs with HF[2], H_2SO_4[3], HF/HCl/HNO_3[4] or HF/HCl[3] at high temperatures is often applied. A dissolution without HF usually requires more than 16h of heating. The use of HF makes the dissolution faster but often requires subsequent removal of the fluoride.

Fusion with $K_2S_2O_7$[5], $LiBO_2/H_3BO_3$[6], $Li_2B_4O_7/Li_2CO_3$[7], $Na_2B_4O_7/H_3BO_3/LiOH$[8] or Na_2O[9] is much less time consuming, however, this requires high temperature($\sim$1000°C), the use of platinum crucibles which can easily lead to contamination and the addition of an excess of reagents which are difficult to purify. These facts renders fusion methods susceptible to losses and contamination. Furthermore, ZrO_2 can be decomposed in an open system by treatment with concentrated H_2SO_4 and $(NH_4)_2SO_4$[10]. A 30 to 40-fold excess of reagents is required and at the temperature used($\sim$200°C) large amount of sulphate remain. This dissolution method is only appropriate for less resistant zirconia materials.

As described by Lobinski *et al*[21], a fusion with NH_4HSO_4 is very effective for sample decomposition in the case of ZrO_2 powders as explained in 4.2. Direct analyses of ZrO_2 without separation of the Zr matrix can be hampered by a number of interferences (eg. sensitive Hf lines were found to be interfered by Zr matrix lines) and also B, Mn, and Ti suffer from background enhancement arising from Zr lines). The presence of Y and Ce, which are often used for stabilizing ZrO_2, may also cause interferences, as found for the determination of Al and Y in the presence of Ce.

Removal of the Zr matrix could be achieved by liquid extraction of the TTA complexes of Zr with MIBK and the residual matrix-free aqueous solution can be analyzed by ICP-AES. Further, Zr could also be removed by precipitation of Zr as $ZrOCl_2$ from an acetone-water mixture and the traces kept in the aqueous phase with

high recovery. The detection limits of analytes with or without matrix removal were found to be similar. This might be partly due to the fact that a gain in power of detection by matrix removal if often counteracted by the introduction of contamination in the matrix removal procedure. This requires special purification of the fluxes and other measures so as to lower the risk of contamination. The results obtained with ICP-AES (eg. Al, Ca, Fe, Mg, Na, Ti and Y) in a number of commercially available ZrO_2 powders after matrix removal agree well with those obtained without matrix removal and with those of direct analyses by slurry nebulization

4.2 Dissolution procedure used

The ZrO_2 powder with the fusion agent(NH_4HSO_4) in a 10-fold excess were placed in quartz tubes. The tubes were then placed in an Al block with 70mm height and 30mm i.d. bores and then inserted in a muffle oven coated with Al foil (such that the tubes were covered by the foil)so as to prevent contamination. 0.3 - 0.4g of ZrO_2 powder was decomposed and heated to dryness at approximately 500°C. The residue was dissolved in either 2ml of 1mol/dm^{-3} HNO_3 or in the mixture of 1ml of 40%HF:10ml H_2O. The solution was then transferred to a 100.00ml volumetric flask, filled up with water and analyzed by ICP-AES.

4.3 Experimental

4.3.1 Instrumentation

A Liberty 220 ICP Emission Spectrometry which was fed the sample with a concentric nebulizer has been used for all measurements. The analyte solutions were fed to the nebulizer with the aid of a dual channel peristaltic pump which also drain the excess liquid from the Stuurman Masters Spray chamber.

4.3.2 Reagents

All the reagents used were supplied by Merck. Standard solutions were prepared from stock solutions containing 1000ug/ml of Fe, Cr, Th, U and Zr. Working standards were freshly prepared by dilution of the stock solution with distilled water. HF and HNO_3 solvents were prepared from the AR grade acids. Ar was used as both the plasma and nebulization gas. NH_4HSO_4 used was of Suprapure quality.

4.3.3 Optimization of the working conditions

The optimization of working conditions that can influence the precision of the determination of the trace impurities in ZrO_2 was carried out in order to obtain the highest values of each parameter. The following parameters were considered:

observation height, nebulizer pressure, integration time, forward power, pump speed, plasma and auxiliary gas flow. The experimentation was carried out by performing consecutive wavelength scans in a ± 0.15nm vicinity of the line and measuring the emission intensity in the peak maximum for each scan. This process was carried out for all analytical lines chosen. The conditions chosen for the determination of the elements are those that give the highest value for the readings of emission intensity. Figure 18 and 19 show how the nebulizer pressure and pump speed were optimized respectively. The optimum conditions used in the analysis are summarised in table 9.

4.3.4 Preparation of standards and calibration

The calibration of the analysis of Cr, Fe, Th, U and Zr in ZrO_2 was carried out by standard addition method. This calibration method was favoured because the matrix of the fused ZrO_2 was not well defined. The calibration curve for the analytes were constructed with the use of 4 standards (viz. Addition 4, Addition 3, Addition 2 and Addition 1) and Addition 0. Addition 0 is the prepared sample without the addition of a standard. The prepared sample and a blank were used for the determination of detection limits for each element.

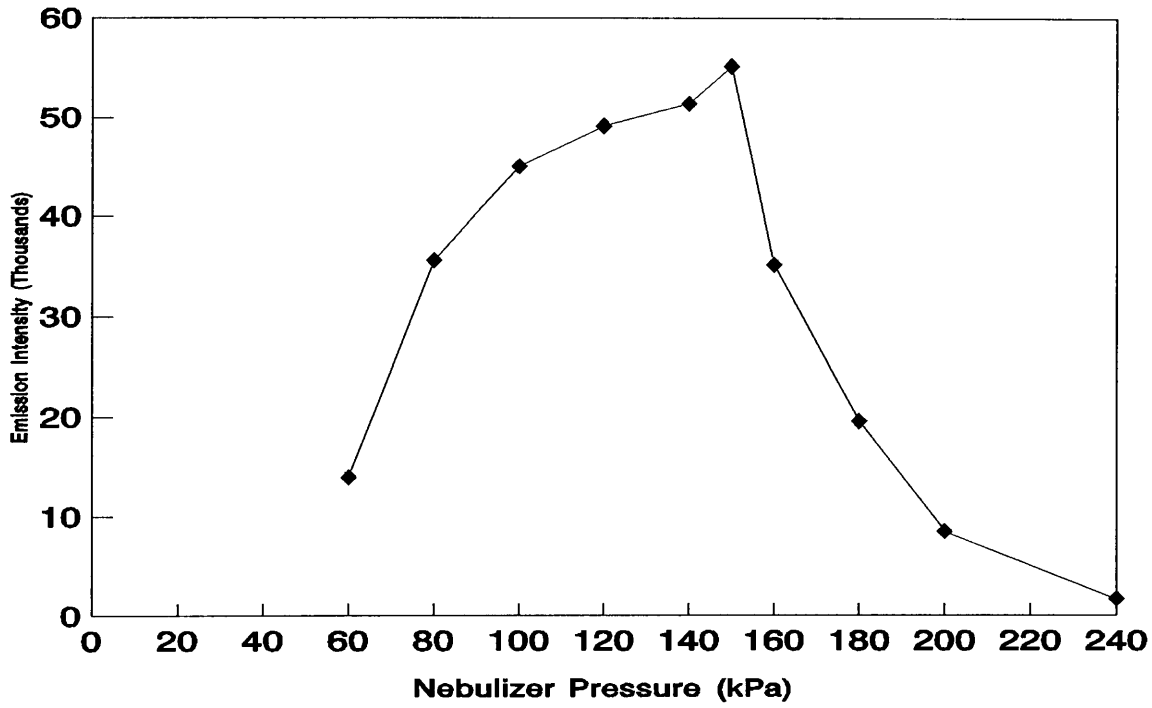

Figure 18. Optimization of the nebulizer pressure using 10μg/ml Fe

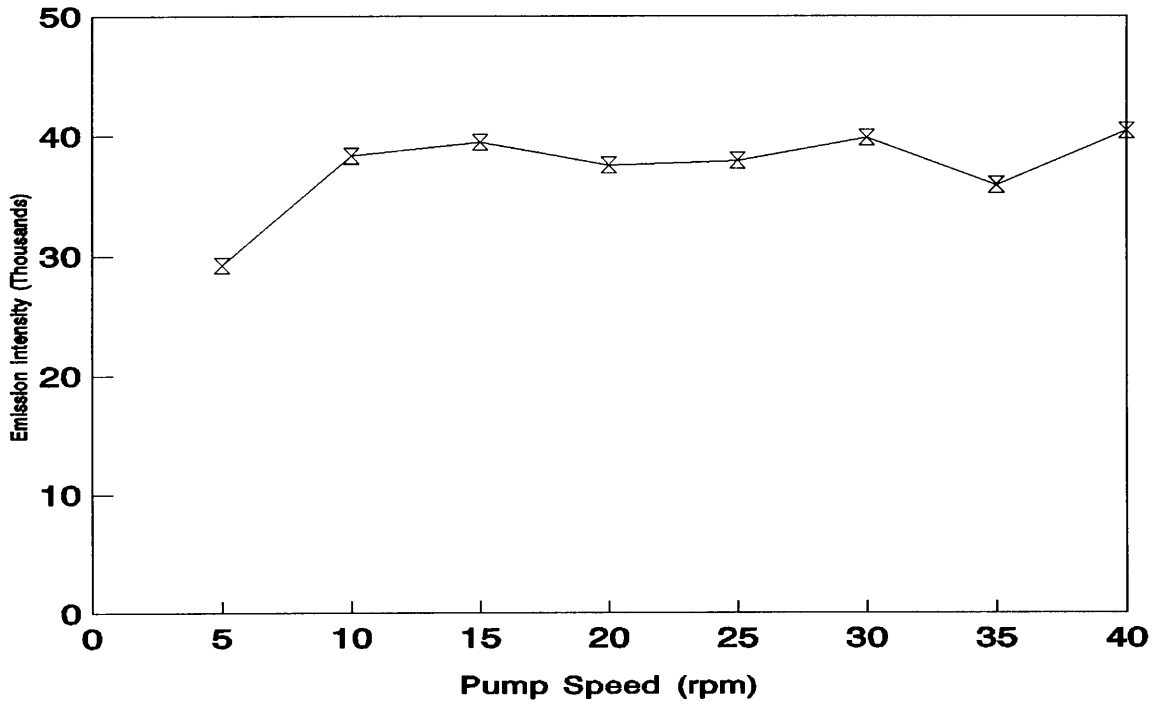

Figure 19. Optimization of the pump speed using 10μg/ml Fe

Table 9 Optimum conditions used

Observation Height/mm	4.00
Integration time/s	8.00
Power/kW	1.00
Plasma gas flow-rate/ l/min	15.0
Auxiliary gas flow-rate/ l/min	1.50
Pump Speed/rpm	15.0

4.4 RESULTS AND DISCUSSION

4.4.1 Decomposition of the samples

The decomposition of the ZrO_2 powder by fusion with NH_4HSO_4 has been preferred because of its rapidity which is supported by results obtained in 3.2 where the digestion of ZrO_2 and evaporation of NH_4HSO_4 were fully completed within 6 hours. Quartz tubes have been preferred over Pt tubes and other vessels as it brings no contamination at concentration levels of the trace elements of interest. NH_4HSO_4 is a suitable flux as it does not attack quartz and is commercially available in suprapure

quality. Moreover, it can be evaporated at a relatively low temperature (~500°C). Hitherto melting with NH_4HSO_4 has been successfully used to collect μg/g amounts of Ti and Zr from biological, environmental and geological materials[11].

4.4.2 Choice of interference free analytical lines for the impurities

Due to the line-rich emission spectrum of Zr a careful choice of analytical lines for the determination of trace impurities is of prime importance. As the line coincidence tables for ICP-AES[12] cover only a limited number of Zr lines and Zr is present at a large excess with respect to the impurities, it is very likely that very weak lines not tabulated emission lines will cause significant spectral interferences.

Line overlap interferences represent the principal limitation of trace analysis by ICP-AES when the analytes must be determined in the presence of high concentration of elements with line-rich emission spectra. The choice of appropriate wavelength for the trace analysis is often difficult owing to the lack of truly comprehensive tables of ICP line intensities.

Plasma spectroscopists are at present forced to use rather brief compilation of "prominent" plasma emission lines[13,14] in combination with much more comprehensive tables for classical atomic emission sources such as the dc arc and ac spark[15 - 17]. Two attempts have been made to put this latter information into a convenient form for use

with ICP-AES[12,18]. Boumans compiled two volumes of line coincidence tables, which is based primarily upon the US National Bureau of Standards tables of spectral line intensities for the copper arc(s).

Use of the classical tables presents a number of some limitation, viz:-

- little information about the relative intensities of ICP emission lines can be obtained, because of the differences in excitation mechanisms in plasmas and those in arcs and sparks.
- many lines observed in plasmas are not listed in the classical tables.
- furthermore, since the data of these tables where obtained almost entirely by photographic plate detection, many ICP lines below 220nm, and particularly those in vacuum UV are missing.

Bouman's N.B.S. copper arc tables also lacks many lines observed in the ICP, and other sources. Furthermore, Winge *et al*[19,20] prepared an Atlas of Spectral Information for ICP-AES. Even though this atlas provide 11 wavelength profiles($\pm$0.15nm) for each 281 prominent lines for 70 elements, no information about possible interferences from elements other than Fe, Al, Ca, Mg, Ti, Cr, Mn, Ni, and V is available.

Criteria for line selection were:

1- Information about the major constituents of the sample (obtained by a preliminary semi-quantitative analysis, if necessary) is used to select one or more potentially suitable lines from the line of coincidence tables.

2- The wavelength profiles of the sample is acquired by making a wavelength Scan. If unanticipated lines are observed (spectral interferences), they are identified if possible, by returning to the tables and performing further scans after the introduction of the certain concentration(s) of the suspected interfering species. If the interfering element has been identified and the spectral interferences are not severe, they can be corrected by interelement correction. If the interferences cannot be avoided, an alternative line must be chosen.

3- the candidate line is accepted to be suitable, depending on the observed interferences which can of course also include background shifts. The line with the lowest background emission signal is chosen. These information is not provided in the line coincidence tables.

In order to choose an interference free line for the analyte, the wavelength scans of the prepared sample was performed for Fe, Cr, Th and U. From these scans, the following lines were chosen:- Fe II 259.940nm, Cr I 359.349nm, Th II 346,992nm and U II 389.036nm. For Zr, the lines were 383.676nm and 327.305nm.

The wavelength selection process for these trace analysis are discussed with reference to experimentally obtained profiles, and to information on potential interferences obtained as supplied by the manufacturer of the instrument.

Wavelength scans for ZrO_2

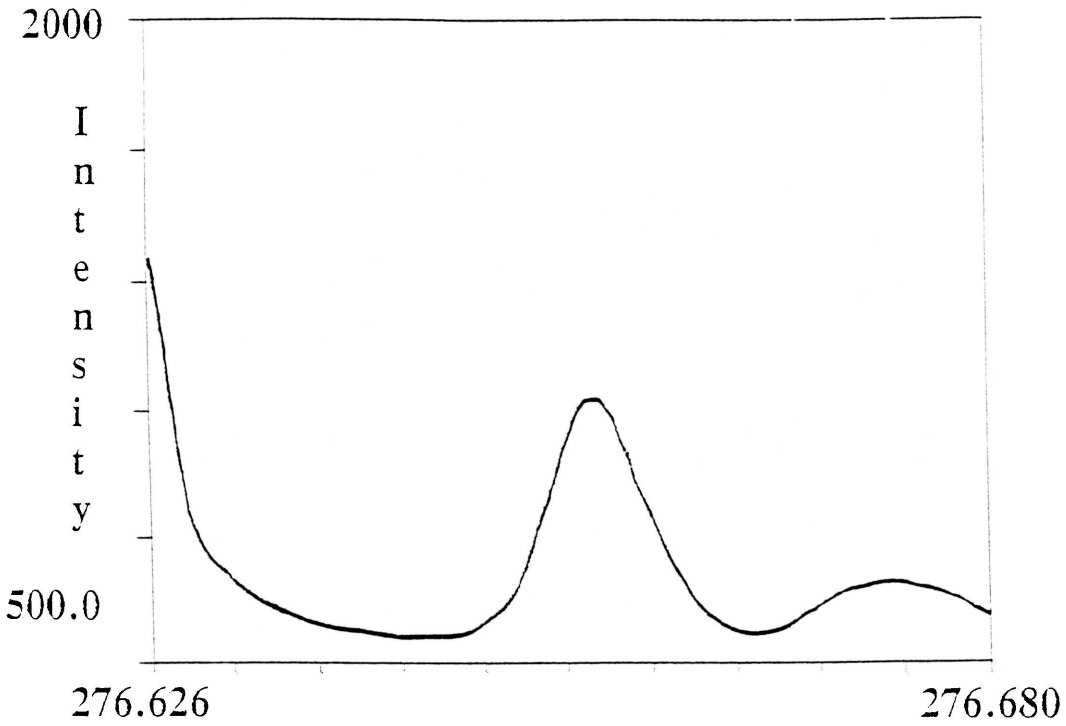

Spectrum 1 Chromium in zirconium oxide at 276.654nm

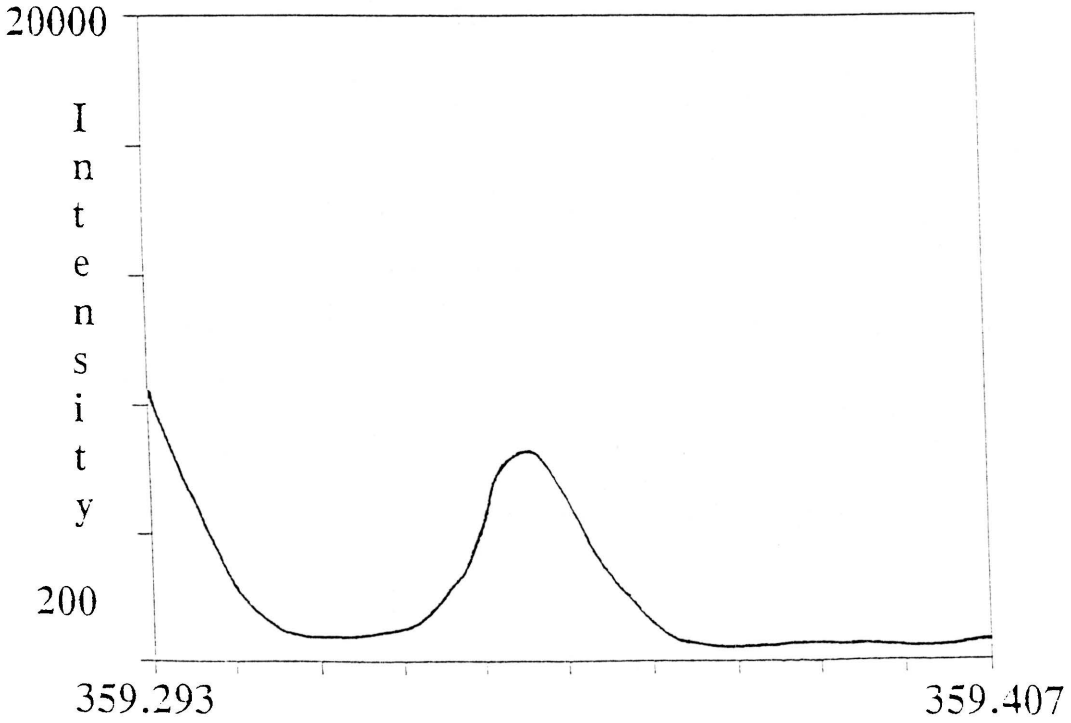

Spectrum 2 Chromium in zirconium oxide at 359.349nm

Wavelength scans for ZrO_2

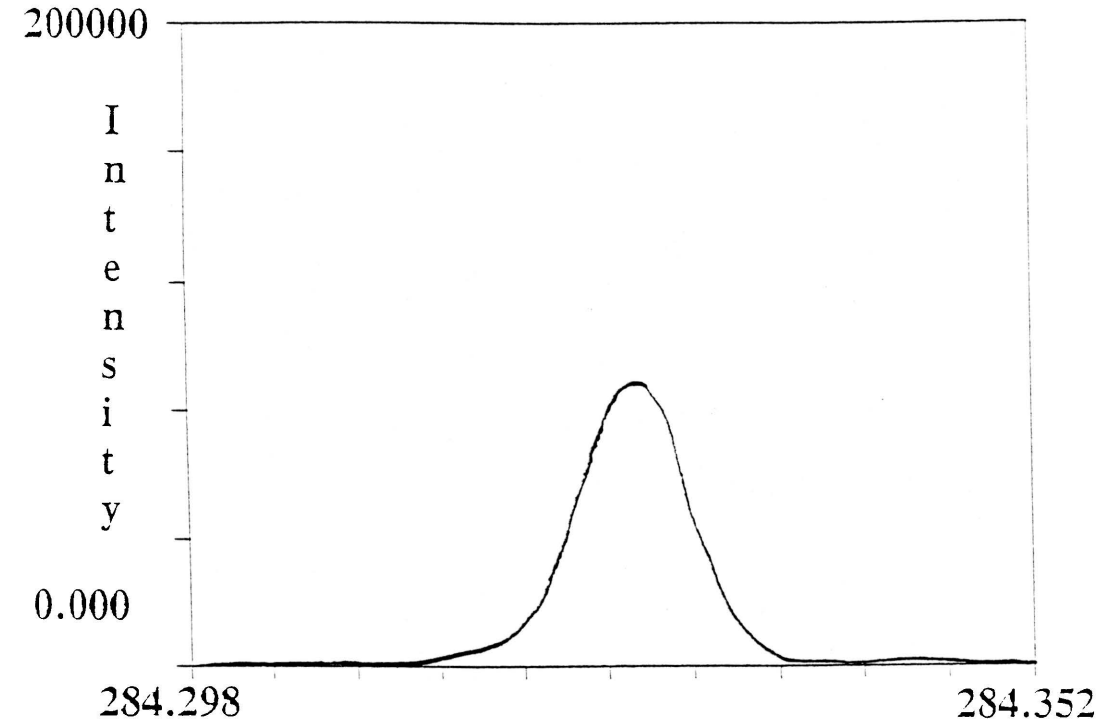

Spectrum 3 Chromium in zirconium oxide at 284.325nm

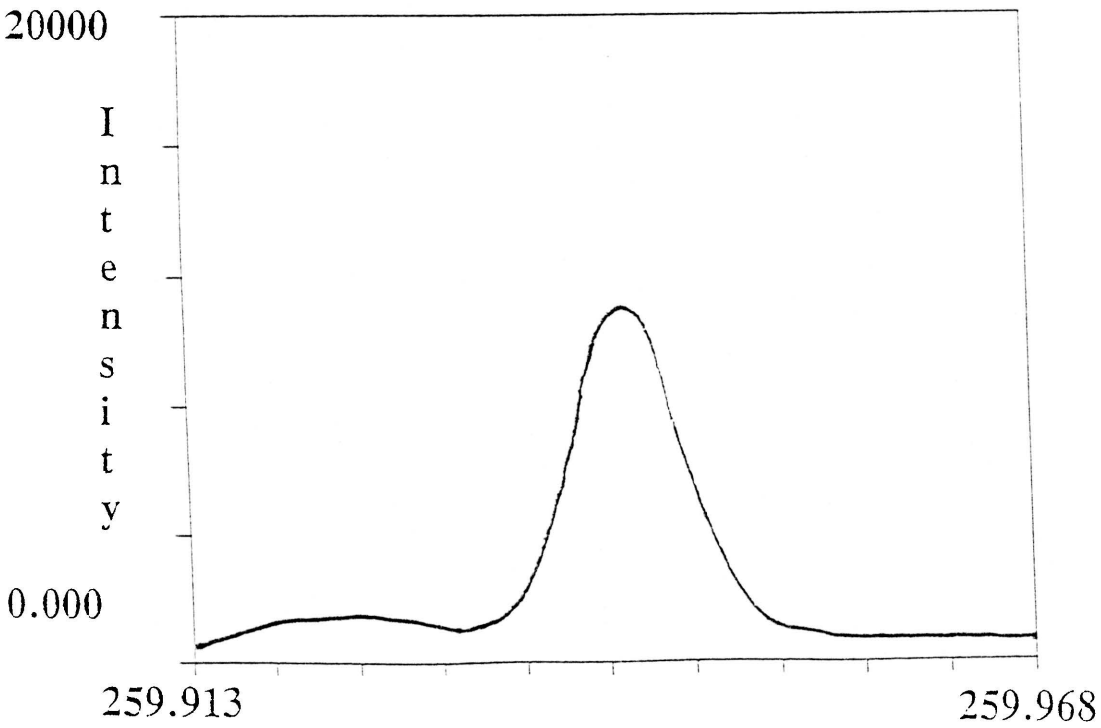

Spectrum 4 Iron in zirconium oxide at 259.940nm

Wavelength scans for ZrO_2

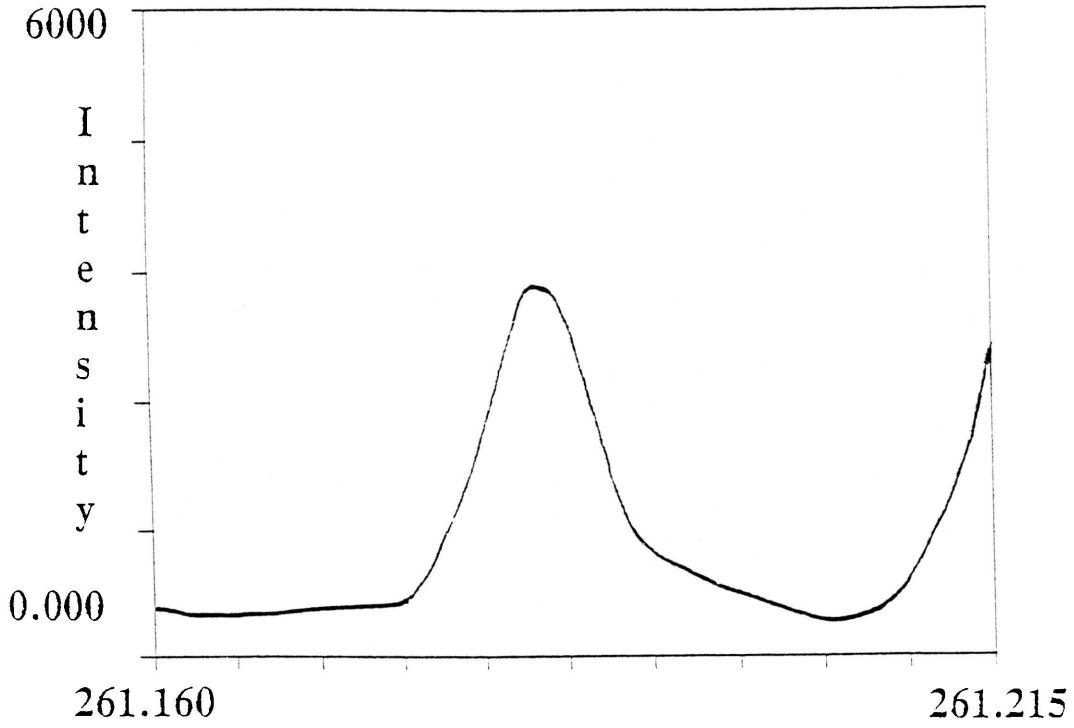

Spectrum 5 Iron in zirconium oxide at 261.187nm

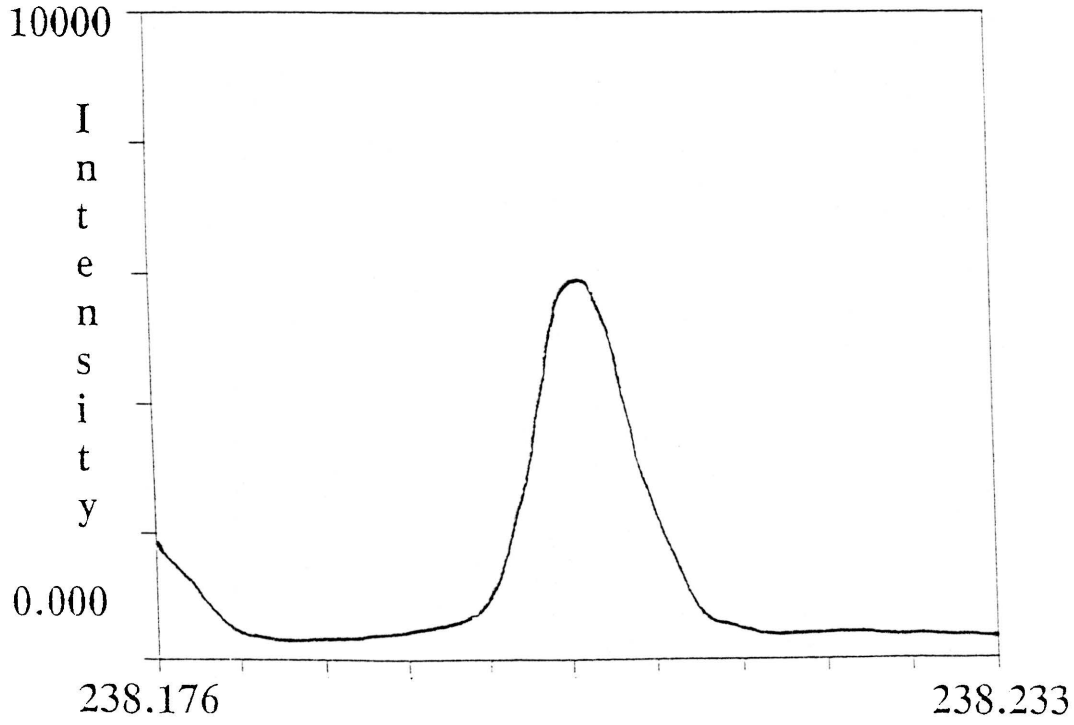

Spectrum 6 Iron in zirconium oxide at 238.204nm

Wavelength scans for ZrO_2

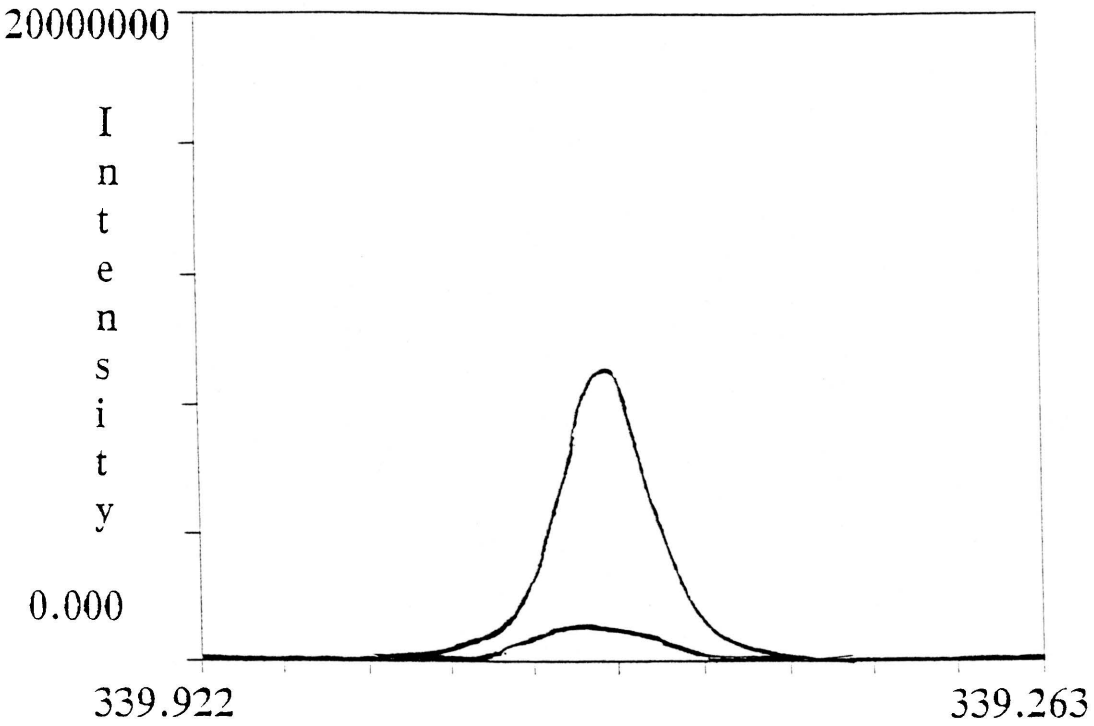

Spectrum 7 Thorium in zirconium oxide at 339.204

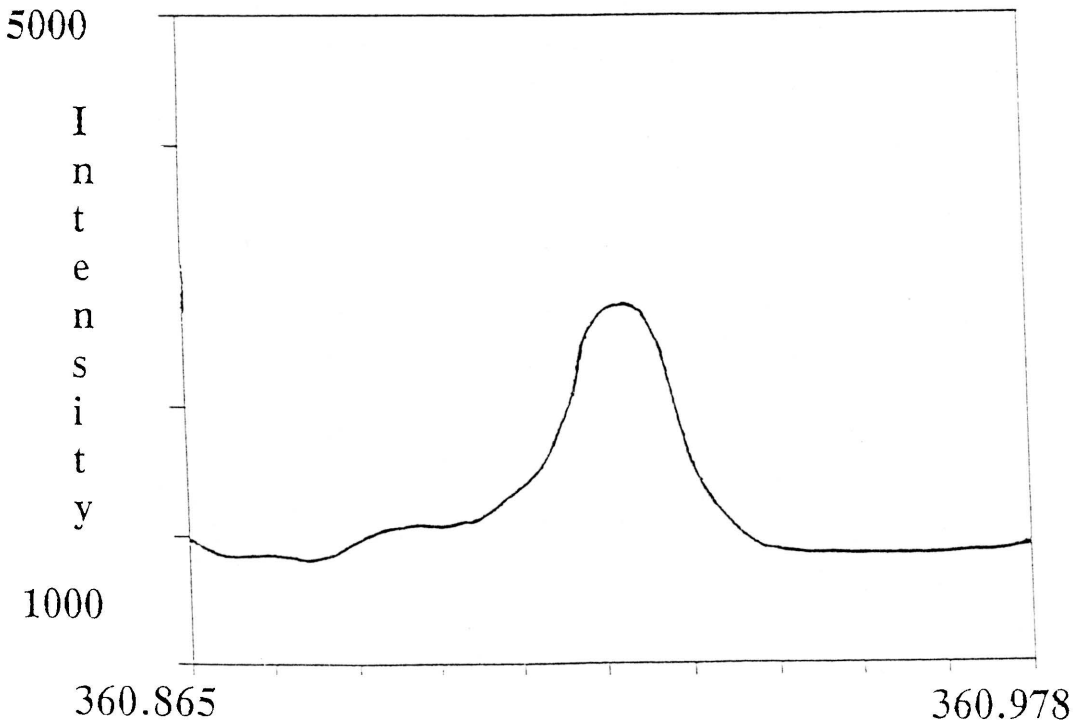

Spectrum 8 Thorium in zirconium oxide at 360.922nm

Wavelength scans for ZrO_2

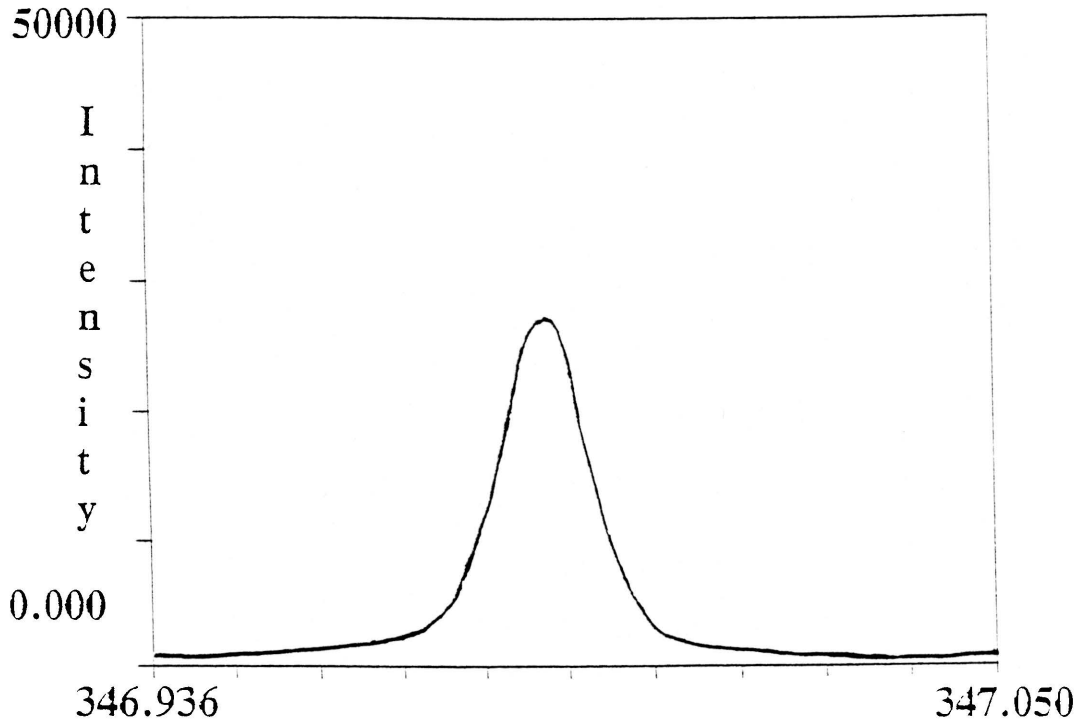

Spectrum 9 Thorium in zirconium oxide at 346.992

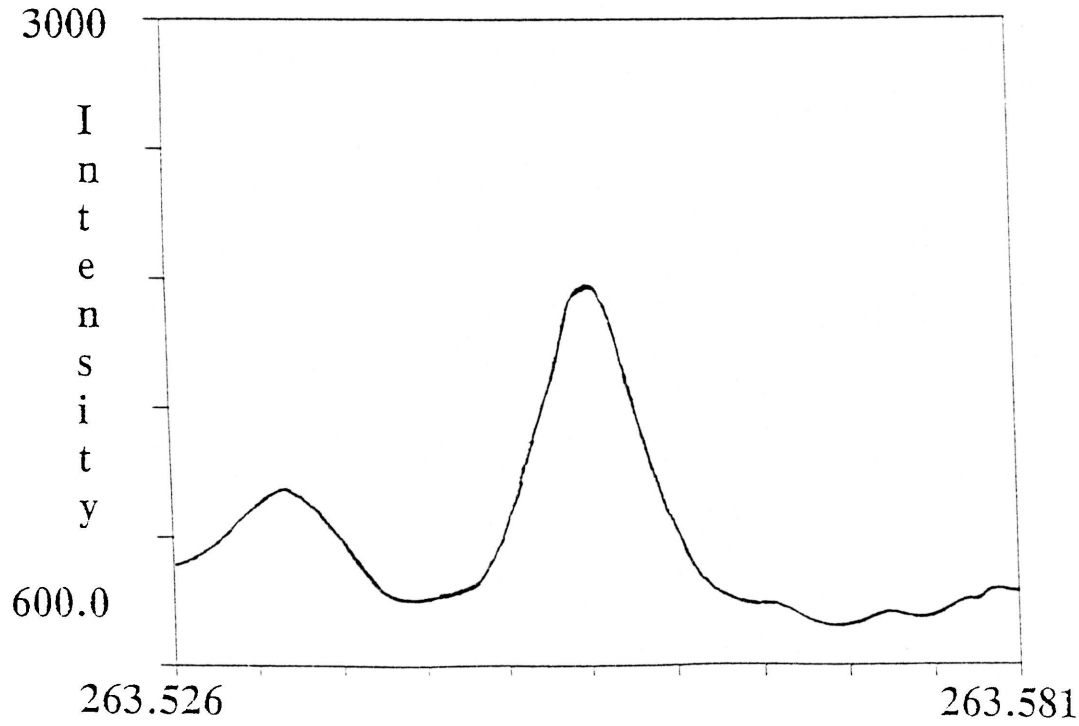

Spectrum 10 Uranium in zirconium oxide at 263.553

Wavelength scans for ZrO_2

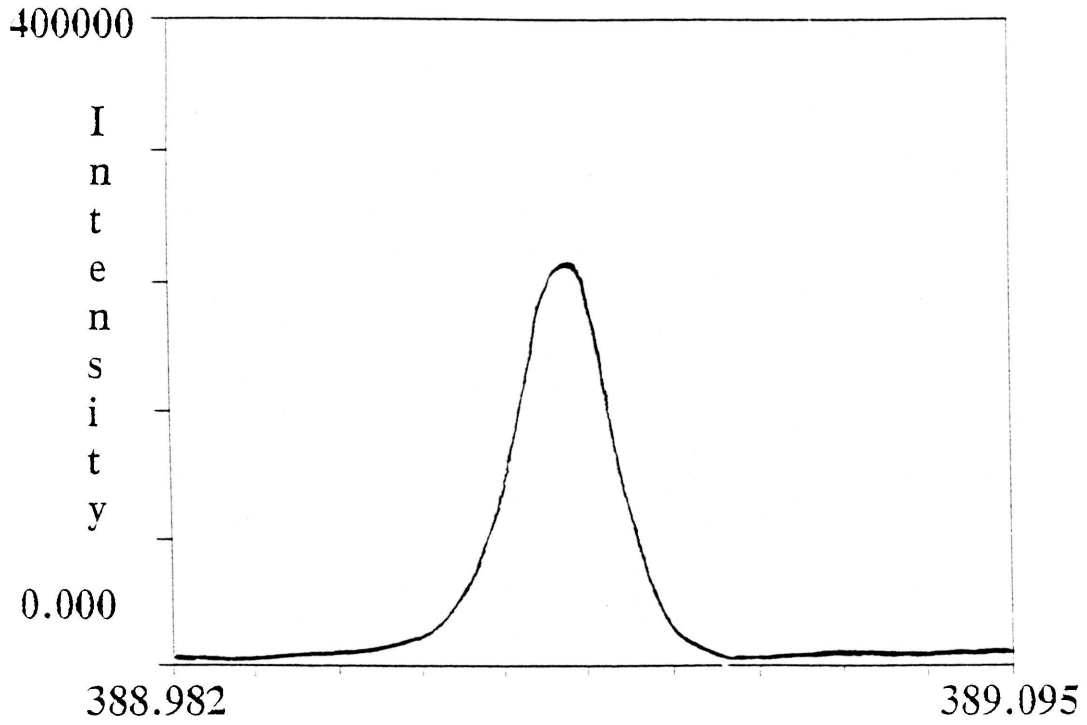

Spectrum 11 Uranium in zirconium oxide at 389.036nm

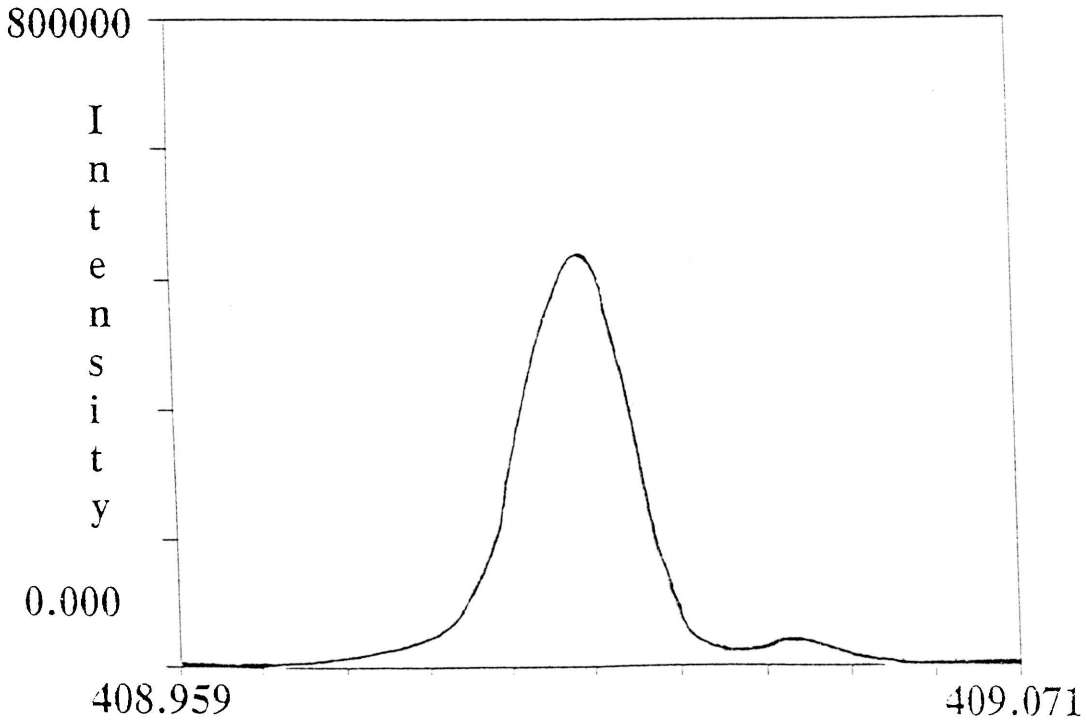

Spectrum 12 Uranium in zirconium oxide at 409.014nm

Wavelength scans for ZrO_2

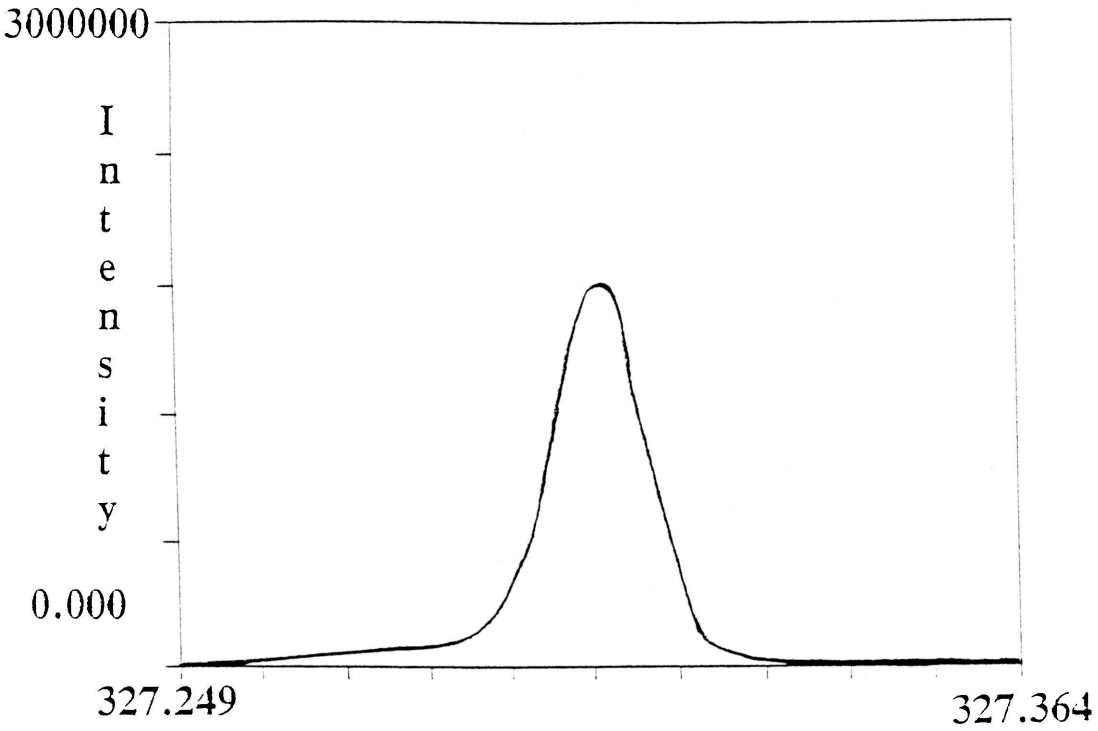

Spectrum 13 Zirconium in zirconium oxide at 327.305nm

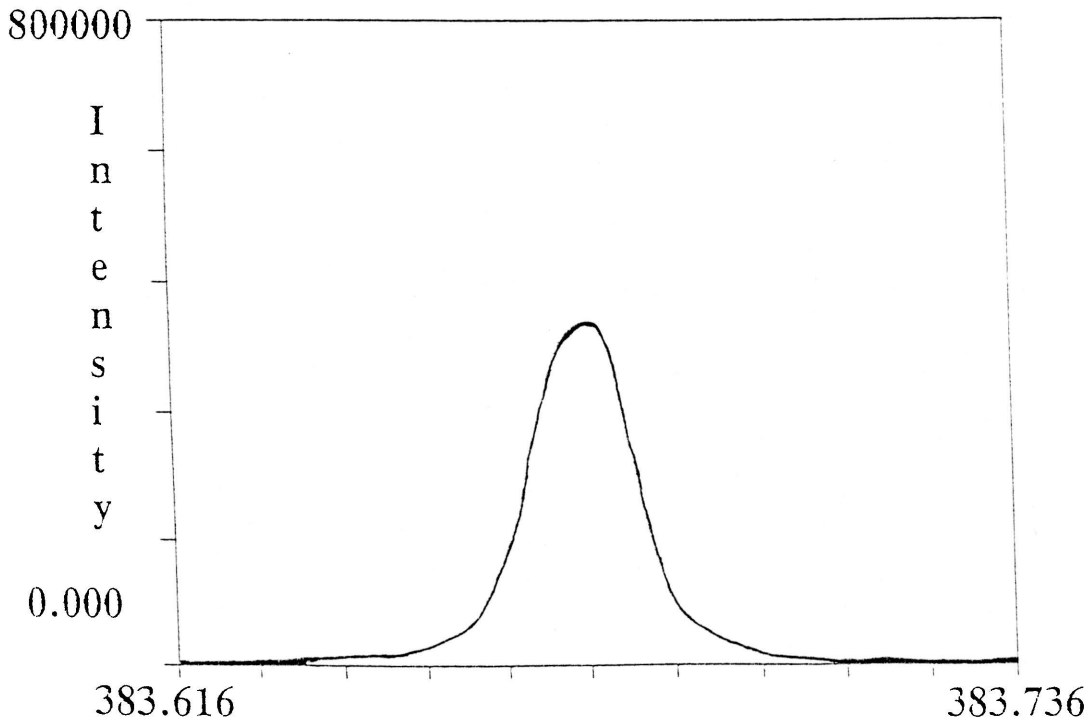

Spectrum 14 Zirconium in zirconium oxide at 383.676nm

Chromium

The determination of chromium in ZrO_2-powders, even at concentrations of 1μg/ml or less is relatively straightforward. Preliminary wavelength profiles revealed moderate peak adjacent to the Cr I 359.249nm line which was eventually identified as Ce II 359.313nm or Ce II 359.323nm. As can be seen from the wavelength scan, this possible interfering peak is far from the Cr peak, i.e. Cr emission signal is not affected. Even though the interference free line Cr II 284.325nm seem to be sensitive and has low background signal, this line cannot be used because it seem to be influenced by the weak Ar line (but Ar is not shown to be an interferent on the list of prominent lines supplied with the instrument) as the emission signal of Cr II 284.325nm remain constant at different concentrations. At the concentration level obtained for Cr in the ZrO_2 samples, Cr II 276.654nm is not a good choice as poor precision is expected from this line due to its lower sensitivity.

Iron

The two most sensitive lines which can be used for the determination of Fe in ZrO_2 are 259.940nm and 238.204nm. A better choice is the FeII 294.940nm despite minor interferences from a much weaker line as Fe II 238.204nm is less sensitive. Fe II 261.187nm suffers from a minor spectral overlap and it is less sensitive than Fe II 259.940nm and Fe II 238.204nm.

Thorium

The determination of Th in variety of ZrO_2 samples is also relatively straightforward. None of the most sensitive line, viz. 360.922nm, 339.204nm and 346.992nm suffers from any spectral interference from another line. Th II 339.204nm is unusable as it is next to the Ar I 339.278nm line which is used as the plasma, nebulizer and auxiliary gas. Determination of Th at this line is not possible as Th emission signal remain constant with change in concentration. Th II 346.992nm is the best line because it is more sensitive than Th II 360.922nm.

Uranium

The determination of U in geological materials, typically at concentration levels of one microgram per millilitre, less or slightly higher, would be difficult even in the absence of variety of interferences on the most sensitive lines due to their high detection limits. As U seem to be existing in ZrO_2 at high concentration levels, its determination posed minor problems. Though U II 409.014nm is the most sensitive line, it suffers from small spectral overlap from Zr II 409.047nm. U II389.036nm line is slightly less sensitive than U II 409.014nm, but it is the best choice as it is free from any spectral interferences and also offers a lower background signal.

EVALUATION OF RESULTS

4.5 Analytical results

The chemical analysis was carried out for the three different ZrO_2 samples [viz. chemical ZrO_2, natural ZrO_2 (baddeleyite) and ZrO_2 (from zircon)], following the optimum working conditions summarised in table 9. The results of the determination of Fe, Cr, Th U and Zr in these samples appear in table 10 - 19. As can be seen, the analytical results obtained for these samples (eg. %recoveries and yield) are in excellent agreement. The concentrations obtained in HF and HNO_3 are in a good agreement although U and Zr concentration are slightly higher than in HNO_3.

4.6 Detection limit and blank values

Detection limits, %recoveries, blank values and %yield of the analyte of samples prepared in HF and HNO_3 are shown in table 10-20. Because detection limits are difficult to measure accurately, each listed value represents the average of ten or more measurements. For the calculation of detection limit, all values represent 3σ detection limits, i.e. they correspond to the concentration of the analyte required to produce a signal intensity equal to three times the standard deviation of the background intensity. It should be emphasized that the power of detection of Fe, Cr, Th, U and Zr is limited by blank contribution rather than by the ICP-background contribution. The summary of the data in table 16 shows that for the lines examined, HF offers slightly lower detection limits than HNO_3. The detection limit of U II 389.036nm was found to be

approximately 0.1μg/ml which is the highest of the impurities in the sample. Therefore, the detection of uranium can only be possible when it is present in significant amounts.

% Yield of U and Zr registered for samples dissolved in HNO_3 were also slightly lower than for samples dissolved in HF. These may either mean that HNO_3 and HF depresses and enhances the emission signals of these two elements respectively. The %recoveries obtained for the analyte elements with the two acids is almost the same. It has been found that there is no significant difference between the blank values of either Fe or Cr in the two solvents. The blank values of U, Th and Zr in HNO_3 are higher than in HF. Due to these, the detection limit of Th and Zr in HNO_3 are slightly higher.

Table 10 The results of determining the % recoveries of Chemical ZrO_2 in HF

Element	Added [μg/ml]	Recovered [μg/ml]	%Recovery
Fe II 259.940nm	-	0.3746	
	2.0	2.03 $\pm$ 0.01	101
	4.0	3.94 $\pm$ 0.03	98.6
	6.0	5.91 $\pm$ 0.04	98.5
	8.0	7.74 $\pm$ 0.04	96.7
Cr I 359.349nm	-		
	4.0	3.95 $\pm$ 0.02	98.8
	6.0	5.96 $\pm$ 0.04	99.4
	8.0	8.07 $\pm$ 0.09	101
	10.0	10.3 $\pm$ 0.10	103
U II 389.036nm	-	22.98	
	20.0	18.2 $\pm$ 0.37	90.8
	40.0	38.0 $\pm$ 0.49	95.0
	60.0	58.9 $\pm$ 0.46	98.1
	60.0	78.7 $\pm$ 0.96	98.3
Th II 346.992nm	-	15.44	
	10.0	10.2 $\pm$ 0.13	102
	20.0	19.6 $\pm$ 0.12	98.1
	30.0	30.9 $\pm$ 0.54	103
	40.0	39.6 $\pm$ 0.56	99.0
Zr II 383.676nm	-	23.59	
	10.0	10.1 $\pm$ 0.07	101
	20.0	20.1 $\pm$ 0.24	100
	30.0	30.2 $\pm$ 0.35	101
	40.0	40.3 $\pm$ 0.21	101
Zr II 327.305nm	-	23.30	
	10.0	10.0 $\pm$ 0.07	100
	20.0	19.9 $\pm$ 0.20	99.4
	30.0	29.8 $\pm$ 0.31	99.3
	40.0	39.7 $\pm$ 0.28	99.2

Table 11 **The results of the determination of %recoveries of the chemical ZrO_2 impurities in HNO_3**

Element	Added [μg/ml]	Recovered [μg/ml]	%Recovery
Fe II 292.940nm	- 2.0 4.0 6.0 8.0	0.3615 1.97 ± 0.01 3.94 ± 0.06 5.85 ± 0.03 7.85 ± 0.04	 97.1 99.2 101 99.3
Cr I 359.349nm	- 4.0 6.0 8.0 8.0	0.5800 3.89 ± 0.03 5.95 ± 0.04 8.12 ± 0.07 9.93 ± 0.09	 97.1 99.2 101 99.3
U II 389.036nm	- 20.0 40.0 60.0 80.0	23.50 19.4 ± 0.19 38.7 ± 0.37 60.6 ± 0.84 81.9 ± 0.43	 96.9 96.0 101 102
Th II 346.992nm	- 10.0 20.0 30.0 40.0	15.44 9.97 ± 0.13 19.6 ± 0.21 30.7 ± 0.24 40.9 ± 0.26	 99.8 98.2 102 102
Zr II 383.676nm	- 10.0 20.0 30.0 40.0	22.03 19.4 ± 0.17 29.5 ± 0.23 40.4 ± 0.37 49.6 ± 0.36	 97.0 98.4 101 99.2
Zr II 327.305nm	- 10.0 20.0 30.0 40.0	20.97 15.0 ± 0.23 28.5 ± 0.43 39.4 ± 0.31 49.6 ± 0.38	 75.8 95.3 98.4 98.5

Table 12 **The results of the determination of %recoveries of impurities in natural ZrO_2 (baddeleyite) in HF**

Element	Added [μg/ml]	Found [μg/ml]	%Recovery
Fe II 259.940nm	- 2.0 4.0 6.0 8.0	0.3395 2.00 ± 0.02 3.98 ± 0.02 6.11 ± 0.03 8.06 ± 0.05	 100 99.4 102 101
Cr I 359.349nm	- 4.0 6.0 8.0 10.0	0.7111 3.83 ± 0.03 5.97 ± 0.06 8.13 ± 0.06 10.2 ± 0.05	 95.7 99.6 102 103
U II 389.036nm	- 20.0 40.0 60.0 80.0	24.82 18.3 ± 0.26 39.5 ± 0.70 59.8 ± 0.47 79.6 ± 0.56	 91.3 98.8 99.7 99.6
Th II 346.992nm	- 10.0 20.0 30.0 40.0	16.53 9.91 ± 0.19 19.6 ± 0.16 28.5 ± 0.26 39.0 ± 0.49	 99.1 97.8 95.0 97.4
Zr II 383.676nm	- 10.0 20.0 30.0 40.0	24.68 9.88 ± 0.24 19.9 ± 0.13 29.5 ± 0.27 40.2 ± 0.29	 98.9 99.4 98.4 101
Zr II 327.305nm	- 10.0 20.0 30.0 40.0	24.66 9.84 ± 0.13 19.7 ± 0.22 29.9 ± 0.30 40.3 ± 0.29	 98.3 98.5 99.8 101

Table 13 **The results of the determination of %recoveries of impurities in natural ZrO_2 (baddeleyite) in HNO_3**

Element	Added [μg/ml]	Found [μg/ml]	%Recoveries
Fe II 259.940nm	-	0.3092	
	2.0	2.03 $\pm$ 0.01	102
	4.0	4.05 $\pm$ 0.02	101
	6.0	5.98 $\pm$ 0.04	99.7
	8.0	8.03 $\pm$ 0.05	100
Cr I 359.349nm	-	0.6160	
	4.0	3.84 $\pm$ 0.04	96.1
	6.0	5.92 $\pm$ 0.05	98.7
	8.0	7.99 $\pm$ 0.04	99.8
	10.0	9.92 $\pm$ 0.09	99.2
U II 389.036nm	-	22.21	
	20.0	20.4 $\pm$ 0.23	102
	40.0	39.5 $\pm$ 0.50	98.6
	60.0	59.9 $\pm$ 0.42	99.9
	80.0	78.9 $\pm$ 0.44	98.6
Th II 346.992nm	-	15.38	
	10.0	9.96 $\pm$ 0.08	99.6
	20.0	20.3 $\pm$ 0.15	102
	30.0	30.1 $\pm$ 0.29	100
	40.0	40.1 $\pm$ 0.31	100
Zr II 383.676nm	-	20.43	
	10.0	10.2 $\pm$ 0.13	102
	20.0	20.9 $\pm$ 0.21	105
	30.0	30.7 $\pm$ 0.29	102
	40.0	39.6 $\pm$ 0.37	99.0
Zr II 327.305nm	-	21.12	
	10.0	9.99 $\pm$ 0.17	99.9
	20.0	20.5 $\pm$ 0.15	102
	30.0	29.6 $\pm$ 0.23	98.7
	40.0	39.0 $\pm$ 0.20	97.6

Table 14 **The results of the determination of %recoveries of impurities in ZrO_2 (from zircon) in HF**

Element	Added [μg/ml]	Found [μg/ml]	%Recoveries
Fe II 294.940nm	-	0.3280	
	2.0	1.98 ± 0.08	99.0
	4.0	3.93 ± 0.02	98.3
	6.0	5.94 ± 0.03	99.0
	8.0	7.90 ± 0.03	98.7
Cr I 359.349nm	-	0.6466	
	4.0	3.88 ± 0.03	97.1
	6.0	5.87 ± 0.05	97.9
	8.0	8.06 ± 0.05	101
	10.0	10.2 ± 0.09	102
U II 389.036nm	-	26.39	
	20.0	18.2 ± 0.27	91.1
	40.0	38.2 ± 0.31	95.4
	60.0	59.5 ± 0.70	99.1
	80.0	80.1 ± 0.51	100
Th II 346.992nm	-	16.54	
	10.0	9.56 ± 0.17	95.6
	20.0	19.6 ± 0.32	97.8
	30.0	30.3 ± 0.32	101
	40.0	40.0 ± 0.49	100
Zr II 383.676nm	-	24.71	
	10.0	9.93 ± 0.21	99.3
	20.0	19.6 ± 0.17	98.1
	30.0	29.2 ± 0.13	97.3
	40.0	39.3 ± 0.36	98.2
Zr II 327.305nm	-	24.06	
	10.0	9.93 ± 0.14	99.3
	20.0	19.5 ± 0.27	97.4
	30.0	29.0 ± 0.32	96.6
	40.0	39.3 ± 0.26	98.1

Table 15 **The results of the determination of %recoveries of trace impurities in ZrO_2 (from zircon) in HNO_3**

Element	Added [μg/ml]	Found [μg/ml]	%Recoveries
Fe II 294.940nm	- 2.0 4.0 6.0 8.0	0.2585 2.02 $\pm$ 0.01 3.84 $\pm$ 0.03 6.07 $\pm$ 0.04 8.26 $\pm$ 0.05	 101 96.0 101 103
Cr I 359.349nm	- 4.0 6.0 8.0 10.0	0.7074 3.84 $\pm$ 0.02 5.89 $\pm$ 0.04 8.01 $\pm$ 0.06 10.1 $\pm$ 0.08	 96.1 98.2 100 100
U II 389.940nm	- 20.0 40.0 60.0 80.0	22.42 20.6 $\pm$ 0.23 39.5 $\pm$ 0.44 59.4 $\pm$ 0.56 80.8 $\pm$ 0.83	 103 98.7 99.1 101
Th II 346.992nm	- 10.0 20.0 30.0 40.0	15.66 9.67 $\pm$ 0.13 19.7 $\pm$ 0.19 29.7 $\pm$ 0.20 38.7 $\pm$ 0.28	 96.7 98.6 99.1 96.7
Zr II 383.676nm	- 10.0 20.0 30.0 40.0	20.91 10.7 $\pm$ 0.18 20.4 $\pm$ 0.10 29.5 $\pm$ 0.38 39.5 $\pm$ 0.28	 107 102 98.2 98.7
Zr II 327.305nm	- 10.0 20.0 30.0 40.0	20.43 9.78 $\pm$ 0.14 20.0 $\pm$ 0.25 29.8 $\pm$ 0.33 39.9 $\pm$ 0.41	 97.8 100 99.3 99.6

Table 16 **Detection limits of the procedures developed for the trace analysis of ZrO_2 powders**

Element	Detection limits [μg/l]					
	HF is the solvent			HNO_3 is the solvent		
	sample 1	sample 2	sample 3	sample 4	sample 5	sample 6
Fe II 259.940nm	1.730	3.840	6.477	3.222	6.2938	5.656
Cr I 359.349nm	9.721	6.974	9.017	14.05	13.01	12.75
U II 389.036nm	69.31	117.5	85.30	135.7	169.1	50.30
Th II 346.992nm	27.83	29.02	17.85	33.12	42.66	47.17
Zr II 383.676nm	19.28	21.67	29.13	15.76	9.090	9.703
Zr II 327.305nm	21.90	11.96	21.46	33.95	33.59	29.99

Table 17 **Blank values in the procedures developed for the analysis of ZrO_2 powder**

Element/nm	Average HF blank intensities	Standard deviation	Average HNO_3 blank intensities	Standard deviation
Fe II 259.940	55.64	3.87	43.29	6.46
Cr I 359.349	33.16	8.38	24.63	3.71
U II 389.036	41.21	9.98	105.3	6.37
Th II 346.992	39.77	5.81	121.0	10.62
Zr II 327.305	113.2	19.17	150.0	16.04
Zr II 383.676	45.88	8.25	365.9	24.03

Table 18 **Comparison of the amount of trace impurities in different types of ZrO_2 samples**

Element	% in Chemical ZrO_2		% in natural ZrO_2 (baddeleyite)		% in ZrO_2 (from Zircon)	
	HF	HNO_3	HF	HNO_3	HF	HNO_3
Fe II 259.940nm	0.03	0.03	0.03	0.03	0.03	0.02
Cr I 359.349nm	0.05	0.05	0.06	0.05	0.05	0.05
Th II 346.992nm	2.37	2.35	2.51	2.34	2.51	2.38
U II 389.036nm	35.1	33.5	37.7	34.0	40.0	34.1
Zr II 327.305nm	71.9	63.8	74.9	64.6	73.0	62.1
Zr II 386.676nm	71.0	68.1	75.3	62.5	75.1	63.4

Table 19 Reference material (ZrO_2)

Element	Added [μg/ml]	Found [μg/ml]	%Recovery
Fe II 259.940nm	-	0.4531\0.3926	
	2.0	1.92 $\pm$ 0.03	96.1
	4.0	4.08 $\pm$ 0.06	102
	6.0	6.18 $\pm$ 0.05	103
	8.0	7.98 $\pm$ 0.10	99.8
Cr I 359.349nm	-	0.9932	
	4.0	4.01 $\pm$ 0.03	100
	6.0	6.21 $\pm$ 0.04	104
	8.0	7.90 $\pm$ 0.06	98.8
	10.0	10.4 $\pm$ 0.08	104
Th II 346.992nm	-	23.04	
	10.0	9.81 $\pm$ 0.15	98.1
	20.0	19.3 $\pm$ 0.15	96.6
	30.0	30.8 $\pm$ 0.39	103
	40.0	37.1 $\pm$ 0.95	92.7
U II 389.036nm	-	17.64	
	20.0	19.3 $\pm$ 0.21	96.5
	40.0	40.4 $\pm$ 0.60	101
	60.0	58.3 $\pm$ 0.56	97.2
	80.0	79.2 $\pm$ 0.71	99.1
Zr II 383.676nm	-	28.46	
	10.0	11.2 $\pm$ 0.29	112
	20.0	19.4 $\pm$ 0.29	96.9
	30.0	30.3 $\pm$ 0.24	101
	40.0	39.9 $\pm$ 0.36	99.7
Zr II 327.305nm	-	27.95	
	10.0	9.56 $\pm$ 0.22	95.6
	20.0	18.8 $\pm$ 0.18	94.2
	30.0	29.2 $\pm$ 0.23	97.8
	40.0	39.9 $\pm$ 0.38	99.7

Table 20 %Yield of trace impurities in the reference ZrO_2 sample

Element	%Yield	Concentration (μg/ml)
Fe II 259.940nm	0.0358	1.4159
Cr I 359.349nm	0.0769	3.104
Th II 346.992nm	3.56	144
U II 389.086nm	21.8	882
Zr II 383.676nm	70.4	2846
Zr II 327.305nm	69.1	2795

4.7 Accuracy and Precision

Unfortunately, standard reference materials have not been analyzed and it is difficult to compare the accuracy of the results obtained using HF and HNO_3. The precision of ZrO_2 samples in HNO_3 is not reproducible day by day. There tend to be a decrease in emission signals of the analyte elements due to the formation of precipitates. ZrO_2 samples in HF are stable as the results are reproducible(with the relative standard deviation of Fe, Cr, Th and U being 0.5, 0.82, 1.60 and 1.20 respectively) and precipitates never forms.

4.8 Interelement interferences

As the results of the analyzed ZrO_2 samples shows Zr/U, Zr/Th, Zr/Cr and Zr/Fe concentration ration to be high, it was necessary to study interelement interferences in the determination of these analytes in the presence of Zr. Interelement effects were studied by measuring the analyte signals for solutions with variable concentrations of Zr and 5μg/ml of the analytes. The interelement effect was defined as the difference between the analyte signals from spiked and unspiked Zr solutions. Figure 20 shows the %relative emission intensity loss of Fe for Zr solutions towards a spiked water. It has been shown that with increasing Zr concentration the analyte signal of Fe decreases considerably.

This agrees well with the observation made by Lobinski *et al*[21] for Fe. For the concomitant/analyte concentration ratio encountered in ZrO_2, it can be confirmed that Zr interferences on Fe are minimum. This has been observed by measuring the signal depression at various Zr matrix concentrations and converting these signals to analyte concentration. For Cr, Th and U, it was not possible to determine Zr's influence on these analytes as the Zr standard was contaminated with these elements.

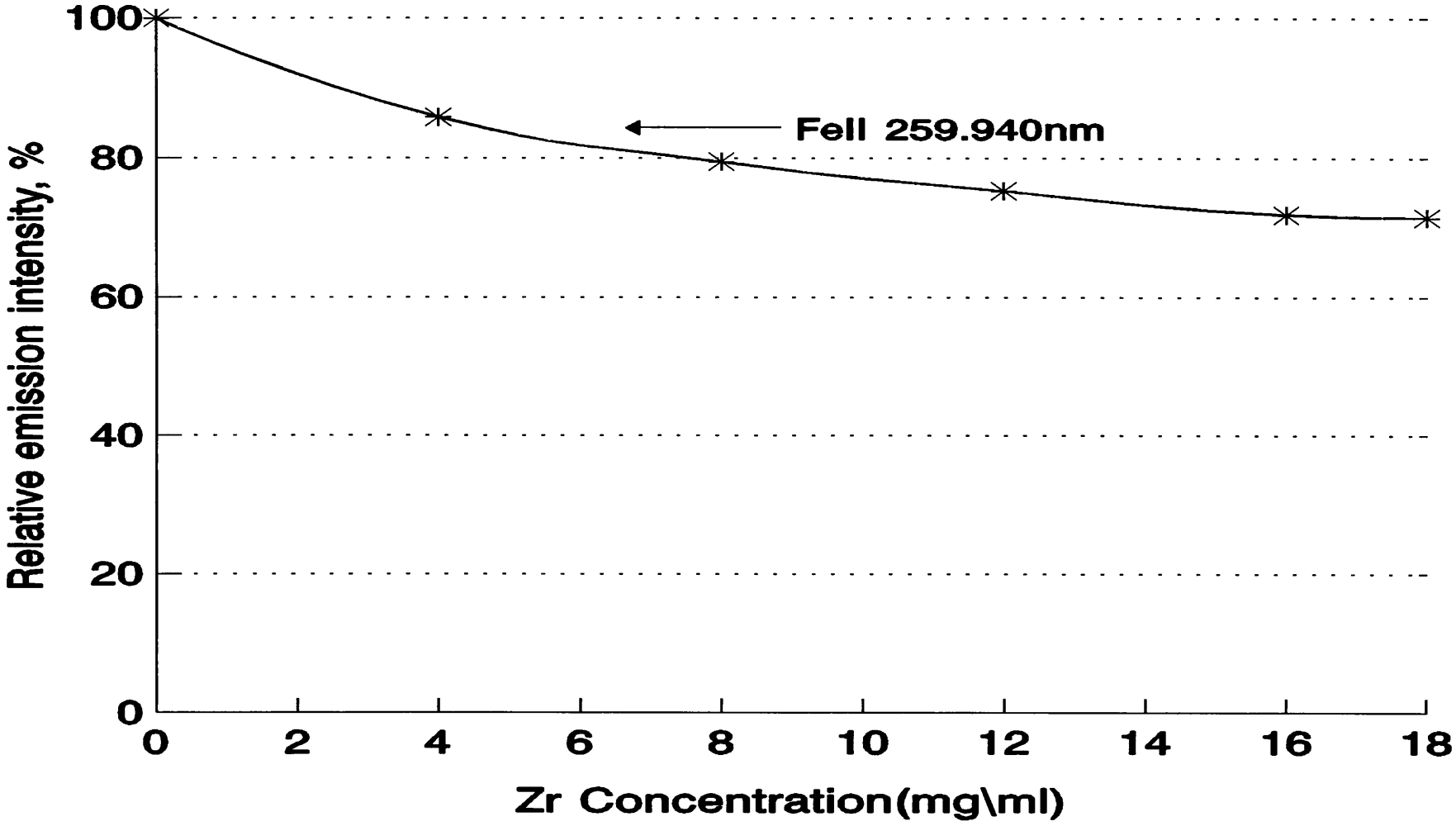

Figure 20. Effect of the Zr concentration on the depression of Fe at 259.94nm

4.9 Conclusion

This study has shown that Fe, Cr, Th and U can be determined in ZrO_2 powders by ICP-AES of the digested sample without separating the matrix(Zr). In this work a decomposition by fusion with NH_4HSO_4 has been preferred because of its rapidity. Moreover, the whole analytical procedure for the determination of trace impurities requires a minimum of manual operation and accordingly the risks for contamination and/or loses of the analytes are minimal as well. With the later aim it appeared advantageous to perform in one vessel.

Quartz has been preferred over Pt and other materials for the vessels for the reasons mentioned in 4.4.1. To estimate to what excess the NH_4HSO_4 flux must be added so as to reliably decompose the ZrO_2 powder, Lobinski *et al*[21] found that at least a 10-fold excess of the reagent(NH_4HSO_4) with respect to ZrO_2 is necessary for obtaining complete sample dissolution. The fusion can be completed in 10-15 minutes and another 30 minutes are required for each 100mg sample mixture to be evaporated to dryness. With such an excess of NH_4HSO_4, the blank expected is considerably lower than with other fluxes.

It can therefore be recommended to dissolve the digested ZrO_2 sample in HF than in HNO_3. ZrO_2 samples which have been dissolved in HF offer lower detection limits and good precision. The detection limits in ZrO_2 in the two acids varied from 1.73μg/l(Fe) to 50μg/l(U). It can therefore be concluded that uranium is determined

efficiently in ZrO_2 only if it is present in significant amount due to its high detection limit. Except for Fe and Cr, the blank values encountered in HF, were lower than HNO_3, but generally, they were below the detection limits. The difference encountered with respect to interferences and accuracy between the two acids is minimum. In order to use HNO_3 as a solvent, the sample must be analyzed immediately after preparation as it seem to be unstable because precipitates forms within days.

As it was shown that Zr depresses Fe emission signal as its concentration increases, (as shown in figure 18), such an effect seems to be related to the excitation energies of the line. It was found by Lobinski *et al*[21] that the effect is larger for the lines with higher excitation potentials. This agrees well with the observation made by Thompson *et al*[22] for Ca. Under stable plasma operating conditions the matrix effects remain constant and reproducible.

4.10 References

4.1 Hickman, D.A., Rooke, J.M., and Thompson, M., J Anal. At. Spectrom., 1986, **1**, 169R

4.2 Stulik, K., Beran, P., Dolezal, J. and Opekar, F., Talanta, 1978, **25**, 363

4.3 Ishizuka, T., Uwamino, Y., and Tsuge, A., Bunseki Kagaku, 1985, **34**, 385

4.4 Van Poucke, L.C., Francois, J.R., and Carleer, R., Bull Soc Chim Belg, 1985, **95**, 385

4.5 Barbina, T.M., and Poleshaev, Y.M., Zavod Lab, 1984, **50(6)**, 12

4.6 Wise, W.M., and Solsky, S.D., Anal Lett, 1976, 1047

4.7 Stephenson, D.A., Anal Chem, 1969, **41**, 966

4.8 Kruidhof, H., Anal Chim Acta, 1978, **99**, 193

4.9 Usmanova, M.M., Yakovskay, T.A., Karamnova, V.S., Kholyavko, E.P., Azovtseva, L.N., and Khodzhamberdyeva, A.A., Zavod Lab, 1981, **47(5)**, 40

4.10 Bastius, H., Ber Dtsch Keram Ges, 1984, **61**, 140

4.11 Matsumoto, K., Misaki, Y., Hayashi, K., and Terada, K., Fresenius Z Anal Chem, 1982, **312**, 542

4.12 Boumans, P.W.M, Line coincidence tables for ICP-AES, Volume 2, Pergamon, Oxford, U.K.

4.13 Winge, R.K., Peterson, V.J., and Fassel, V.A., Appl. Spectrosc., Acta, 1979, **33**, 206

4.14 Boumans, P.W.J.M, and Bosveld, M., Spectrochim. Acta., **34B**, 59

4.15 Harrison, G.R., Massachusets of Technology wavelength Tables, M.I.I. Press, 1969, Cambridge, MA., USA

4.16 Zaidel, A.N., Prokof'ev, and Raiskii, S.M., Tables of Spectrum lines, 1961, Pergamon Press, Oxford, UK

4.17 Meggers, W.F., Corliss, C.H., and Scribner, B.F., Tables of Spectral-line Intensities, 1975, 2nd edn, N.B.S. Monograph 145. U.S. Dept. of Commerce, National Bureau of Standards, Washington

4.18 Parsons, M.L., Forster, A., and Anderson, D., An Atlas of Spectral interferences in ICP Spectroscopy, 1980, Plenum Press, New York

4.19 Winge, R.K., Fassel, V.J., and Floyd, M.A., Atlas of Spectral information for

ICP-AES, under review for publication, 1982

4.20 Winge, R.K., Fassel, V.A., Petterson, V.J., and Floyd, M.A., Appl. Spectrosc., 1982, **36**, 210

4.21 Lobinski, R., Broekaert, A.C., Tschopel, P., and Tolg, G., Fresenius J Anal Chem, 1992, **342**, 569

4.22 Thompson, M., and Ramsey, M.H., Analyst, 1985, **110**, 1413

5. General Conclusion

The driving force of this work was the need to improve the quality of analytical measurements made by Inductively Coupled Plasma-Optical Emission Spectrometry (ICP-OES) as applied in the analysis of ZrO_2. ICP-OES, because of its speed, sensitivity and multi-element capabilities has, over the past years, become one of the most popular analytical techniques for the determination of many elements in a wide variety of matrices. Its benefits have made it the mainstay of many analytical laboratories in the environmental, health and general industrial areas.

However, as with the other spectroscopic methods that preceded plasma spectroscopy, there remains the worry about the accuracy of the measurements. The quality of a measurement depends not only on its precision but also on its closeness to the truth,i.e its accuracy. There are many well used procedures for improving accuracy and estimating the "true" answer when faced with matrix problems, e.g standard addition, internal standardization and matrix matching. All these methods are capable of producing improvements in accuracy but problems can still be encountered in application of the techniques.

After the conception of ICP-OES as an analytical method, its applicability for wide variety of sample types and matrices was very high compared to other techniques, viz. flame and arc/spark spectroscopy. Historically the two main techniques, flame and arc/spark spectroscopy, proved to be excellent in uncertain applications but limited in

others. Flame spectroscopy, is simple to use and provides rapid, quantitative analysis but is limited in the range of elements that can be determined due to the use of a relatively low temperature flame as the excitation source. Arc/spark spectroscopy, using a far higher temperature excitation source, can access a far wide set of elements but in its basic form is essentially qualitative or semi-qualitative. Both techniques suffer from other quite serious drawbacks. In the ICP-OES, where the low temperature flame is replaced by a high temperature argon plasma as the excitation source plus the use of vacuum optics, made the technique applicable for most (if not all) elements. Samples can be introduced as liquids using standard nebulization techniques or as solids using "slurries". Sensitive electronic detection systems allowed precise measurement of emission intensities producing low detection limits (μg/l range for some elements). Powerful computer software enables rapid and reproducible wavelength changes making multi-element analysis simple. These advantages plus the already well known benefits of temperature emission spectroscopy such as:

-large linear dynamic range(up to 5 or 6 orders of magnitude)

-relatively small interelement matrix effects

-high precision

all made ICP-OES the favoured technique for multi-element analysis in a wide range of application areas. The technique also lent itself well to automation, making the analysis of large numbers of samples relatively easy. Thus the technique gained popularity in areas such as environmental, hospital and process laboratories.

One of the perceived advantages of ICP-OES is the relative freedom from matrix interferences. As the technique became more widespread and a wider variety of

sample types analyzed, the extent of interference problems in ICP-OES was discovered. It is true to say that interference problems are not severe as in other atomic emission techniques, but they still exist and present a significant problem when trying to achieve the sensitivity that ICP-OES offers.

Inter-element(matrix) interferences in ICP Optical Emission Spectrometry arise from several sources and are still only partially characterised. However, it is now well known that the introduction of alkali metals or other easily ionizable elements(EIE) causes a spatial shift and/or a change in emission intensity from both neutral atoms and atomic ions in the ICP. Depending on the observation location, such changes can result in either positive or negative errors during an analysis. Other elements, less easily ionized(NON-EIE), can also cause errors. It was also shown recently that intact droplets or the vapour clouds that result from them survive to points in the ICP and no doubt affect sample atomization, ionization and excitation. It would be surprising if droplet-related events were not linked in some way to matrix interferences.

It is not yet clear how a concomitant species(EIE or NON-EIE) influences the emission strength or pattern of an analyte element. For example, an added element or electrons it releases upon ionization might alter any of several things:-

- the manner by which energy is coupled into the plasma
- the rate of propagation of such energy throughout the plasma and therefore the plasma structure itself, and
- the coupling of the plasma energy with a sample aerosol to atomize it, with

sample atoms to ionize or excite them or with sample ions to excite them.

Importantly, no matter which of these events is affected by a concomitant species, it would be tied in some way to one or more of the three fundamental parameters in the plasma: the Ar gas flow-rate, the observation height and the gas temperature(power). Consequently, much can be learned about the ICP and how it interacts with a sample by characterizing these three parameters. Of course, because the ICP is highly heterogenous, the three variables must be mapped spatially.

As reported in chapter 3, the presence of mineral acid(s), viz HCl, HNO_3 and/or H_2SO_4, either decreases or increases the emission intensities of an element. The extent of the effects differ from one acid to the other. The use of high HCl, HNO_3 and H_2SO_4 acid concentrations(0-50%(v/v) can lead to a bias in the determination of Fe concentrations. [HCl] and [HNO_3] has little effect on the emission signal of Fe whereas [H_2SO_4] depresses it severely for all concentrations. Addition of H_2SO_4 to a non-acidified solution is certainly to be avoided. An acid concentration of approximately 0.5%(v/v) H_2SO_4 is necessary to obtain a better control of the acid concentration.

It was shown that the depressant or the enhancement effect caused by the presence of these acids is not caused by the solvent transport efficiency. These enhancement or depressive effect cannot be explained by any physical change in the aerosol characteristics(e.g droplet size distribution, nebulizer and transport efficiency) but

rather by variation of the chemical properties of the aerosol.

The reasons prompting the investigation in chapter 4 are centred around the industrial need to analyze ZrO_2 samples for their metal content in a rapid, reliable manner by ICP-OES. Dissolution of ZrO_2 powders by fusion with NH_4HSO_4 has been favoured as it is rapid and NH_4HSO_4 can be evaporated at very low temperature ($\sim 500°C$). Fusion with other flux, ($K_2S_2O_7$, $LiBO_2/H_3BO_3$, N_2O, etc), requires very high temperature(~ 1000).

HNO_3 is not a suitable acid to dissolve the fused ZrO_2. Digested sample dissolved in HNO_3 forms precipitates within days of preparation. This acid can therefore be only used if the samples will be analyzed immediately after preparation to avoid bias in the results. Therefore it is advisable to dissolve the fused ZrO_2 in HF as they are stable and precipitates never forms. The concentration of HF in the prepared ZrO_2 must not exceed 1%(v/v) as HF depresses the emission signal of most elements. HNO_3 may just be used in place of HF if plastic or quartz containers (e.g volumetric flasks) are not available. The storage of ZrO_2 samples dissolved in HF in glasswares, must be avoided as it can lead to contamination because HF attacks glass.

The line rich ICP emission spectrum of ZrO_2 imply severe interference problems. These limitation may be overcomed by using atomic emission spectrometer of high spectral resolution. All the analyte lines used were free from interferences. Zr's matrix effects on analyte elements may be avoided by chemical separation procedures, eg.

solvent extraction, precipitation, etc. Such methods of chemical separation may also lead to the loss of some analyte elements and contamination.

The comparison shown from table 10 to table 18 illustrates the promise HF holds as a solvent for the fused ZrO_2. HF offers slightly lower detection limits for most elements. The detection limits in HF varied from 1.7μ0g/l(Fe) to 69μg/l(U). Despite the defects that HNO_3 is an unstable solvent for ZrO_2, the detection limits, %recoveries, blank values and %yield of some analyte elements are consistently compared well with those in HF. Zr interferences on the analytes may be minimum as shown by the Fe analytical line. If any type of fused ZrO_2 material forms stable solution in HF, i.e no precipitates forms, there would seem to be every hope that it could fulfil problem encountered with HNO_3.